Chapter VI
Structures of Magnetic Fields in the Universe and Galaxies

Mitsuaki FUJIMOTO, Kin-aki KAWABATA and Yoshiaki SOFUE

Department of Physics, Nagoya University, Nagoya

Statistical analyses are made of ninety eight polarized extragalactic radio sources with known redshifts and rotation measures of the Faraday rotation. Distribution diagrams of the rotation measures and the redshifts reveal substantial contributions of a metagalactic magnetic field to the observed Faraday rotations for distant sources. The most probable direction of the metagalactic magnetic field is determined as $l=110°$, $b=15°$ by using sixty one radio sources of $|b|\geq35°$ selected out of these ninety eight data, where l and b denote new galactic longitude and latitude, and the polarized radio waves from the sources of $|b|\geq35°$ have comparatively small galactic Faraday rotation effects. It is concluded that a large-scale metagalactic magnetic field is uniform at least up to a distance of $z=2$ and the field strength is 2×10^{-9} gauss if $N_e=10^{-5}$ electrons cm^{-3} in the metagalactic space. Some upper limits on the amount of antimatter have been obtained from these results and it is concluded that the universe up to $z=2$ is largely deviated from symmetry with respect to matter and antimatter.

The existence of metagalactic magnetic field and recent theories on formation of galaxies suggest that magnetic fields in the Galaxy and galaxies are due to the frozen-in nature of the metagalactic magnetic field in condensing protogalaxies. Magnetic field structures at the level of the Galaxy and galaxies are also discussed.

A circular arm with elliptical cross-section is used as a model of the spiral arm, and it is shown that interstellar gas may flow in a helical path along the axis of the arm. Interstellar helical magnetic lines of force can be in a stationary state, if such non-circular (rolling) motions of gas are superposed on galactic rotation. On the basis of the λ21-cm line survey of galactic plane by Westerhout (1966, 1969), we have searched for the dynamically postulated rolling motion. Distribution diagrams of the rolling motion along the arm suggest that the helical magnetic field is generated where the rolling motion changes its magnitude rapidly along the arm.

Magnetic field topologies in the Magellanic-type barred galaxy are investigated from a magneto-hydrodynamical point of view and are compared with recently measured E-vectors of polarized starlight from the Large Magellanic Cloud. It seems very probable that a magnetized interstellar gas performs a large-scale circulation in the bar and magnetic lines of force are parallel to the stream lines.

Contents

§1. Introduction

1-1 *Historical review*

Magnetic fields in most astronomical systems up to the galactic scale have been a subject of observational study over the past two decades, but their origin on each level remains largely obscure. As Cowling (1945, 1953) has pointed out, the size and electrical conductivity of astronomical systems are so large that primordial magnetic fields entrapped in the systems would not decay significantly in the life of the universe. This simple argument leads us to the belief that the magnetic fields in each system have their origin in the preceding larger systems. Stellar magnetic fields have been associated with the general interstellar magnetic field and galactic magnetic fields with the intergalactic magnetic field. The ultimate origin of the latter is taken to be a primordial magnetic field associated with the early universe.

However, magnetic fields presently existing in each astronomical system

must be considerably distorted by magneto-hydrodynamical effects in the system. For instance, field structure in a galaxy must be subject to magneto-hydrodynamical effects of interstellar gas in the galaxy. Thus in order to get such an explanation about whether the origin of magnetic fields is adequate or not, closer examinations of the magnetic field configurations in each system and of all their implications would be required.

The first observational step to the magnetic field structure in the Galaxy has been made by polarization measurements of starlight and it has been indicated that the magnetic field projected onto a plane perpendicular to the ling-of-sight is nearly parallel to galactic plane and is distributed in a random way in the direction parallel to the spiral arm (Hiltner 1949, 1951, 1956; Davis and Greenstein 1951). On the basis of this fact, Chandrasekhar and Fermi (1953) have proposed a gaseous cylinder as a model of the arm, in which the magnetic line of force runs parallel to the axis of the arm. This cylinder model has been taken for some time as representing a most realistic field configuration, and observed fluctuations in the polarization plane of starlight (Shajn 1956) have been accounted for by the random motion of magnetized interstellar gas.

Since then, using optical polarization data, Behr (1959), Hoyle and Ireland (1961), Ireland (1961) and Stępień (1964) have suggested a helical magnetic field structure. However, the models have not been so persuasive, because the data at that time were concerned only with the magnetic field projected onto a plane perpendicular to the line-of-sight, and there was no definite reason to postulate a helical structure in the magnetic field.

Meanwhile the discovery of linear polarization of emissions from some extragalactic radio sources has confirmed the synchrotron mechanism of emissions, and the subsequent discoveries of the Faraday rotation of the polarization planes (Cooper and Price 1962 and Gardner and Whiteoak 1963) have given a new method of determining longitudinal components of magnetic fields in the medium between the source and the observer, and it has made a remarkable contribution to investigations of magnetic field in the Galaxy. Indeed, the magneto-ionic theory shows that the polarization angle is linearly proportional to square of the wave length when the intrinsic polarization angle at the source is the same for all wave length we observe, and the constant of the proportionality, the rotation measure R.M., is given by

$$\text{R.M.} = 8.1 \times 10^{5} \int N_{e} B_{/\!/} dL \text{ rad m}^{-2}, \tag{1·1}$$

where N_e is the electron number density cm^{-3}, $B_{/\!/}$ is the longitudinal component of the magnetic field in Gauss, and dL is in parsec. When $B_{/\!/}$ is directed to observer, we take it as positive and therefore, we have $\text{R.M.} > 0$.

Earlier investigations (Gardner and Whiteoak 1963 and Gardner 1963)

have already shown that radio sources with large rotation measures are strongly concentrated in the galactic plane, and they have confirmed that the Faraday rotation of these radio sources is mainly due to a magnetized plasma in the Galaxy. Morris and Berge (1964) and Gardner and Davies (1966) have attributed the Faraday rotation to the magnetic field within the local spiral arm of the Galaxy, by showing a large-scale order imposed on the distribution of rotation measures in galactic coordinates.

A great deal of credit is now given to the model of helical magnetic field when the distribution of sign and magnitude of rotation measures of polarized extragalactic radio sources is obtained over the sky, and particularly when the line-of-sight component of the magnetic field is found to be opposite above and below the galactic plane in the longitude ranges $l \approx 20° \sim 80°$ and $l \approx 240° \sim 320°$ (Morris and Berge 1964; Gardner and Davies 1966; Berge and Seielstad 1967). On the basis of these data, Hornby (1966), Bingham and Shakeshaft (1967) have also constructed more realistic models in which helices are tightly wound and sheared through an angle of 40°, counterclockwise seen from the galactic northpole. Mathewson (1968) has carried out extensive polarization measurements for 1400 stars within 500 pc in the southern hemisphere. Combining his observational data and the optical polarization measurements of stars made so far in the northern hemisphere, he has succeeded in obtaining conclusive evidence for the helical magnetic field in the solar neighborhood.

No direct measurement of the topology of magnetic fields had been made in the external "quiet" galaxies beyond the Galaxy, until Visvanathan (1966) observed polarizations of starlight from the Large Magellanic Cloud (LMC). Recently Mathewson and Ford (1970) and Schmidt (1970) have made polarization observations of stars and emission regions in the LMC and the Small Magellanic Cloud (SMC) and also in a gigantic space enveloping these two nebulae. These observations supply many important materials to dynamics of gas in the Magellanic-type barred galaxy and in the space enveloping it, although no theoretical works have been made about them. Among them it is interesting to note that magnetic lines of force in the LMC are, if we follow Davis and Greenstein (1951), roughly parallel to the bar (Mathewson and Ford 1970) and they are also parallel to the line joining the LMC and the SMC in the space enveloping these two nebulae (Schmidt 1970).

Far beyond the level of galaxies, we have no definite knowledge of magnetic fields except for purely theoretical speculations of a possible primordial magnetic field on cosmological scale.

Ginzburg and Syrovatskii (1964) have proposed a promising method of detecting intergalactic magnetic fields directly by use of the Faraday rotation of polarized extragalactic radio sources, although no observational conclusions have been obtained so far. However, new statistical analyses are made on

distant polarized radio sources with known redshifts (Sofue, Fujimoto and Kawabata 1968, and Kawabata, Fujimoto, Sofue and Fukui 1969), and evidence has been obtained that the metagalactic magnetic field may be responsible for the observed Faraday rotation for radio sources with large redshift z and at intermediate and high galactic latitudes. They have inferred a presence of a large-scale metagalactic magnetic field of 2×10^{-9} gauss (if $N_e = 10^{-5}$ cm^{-3}), uniform up to a distance of $z = 1.4$. The similar investigations have been made by Reinhardt and Thiel (1970) and Reinhardt (1971a) using twice as much as data, and Reinhardt and Thiel have supported these results.

Thus a primordial magnetic field on a cosmological scale seems to be in a scope of physics and it is one of the principal subjects of the present paper.

1-2 *Subjects of the present paper*

On the basis of the recently extended list of extragalactic radio sources of known rotation measures and redshifts, we reexamine in §2 the presence of a large-scale metagalactic magnetic field. The method to analyze the data is essentially the same as developed before by Sofue, Fujimoto and Kawabata (1968) and Kawabata, Fujimoto, Sofue and Fukui (1969); as the distance of extragalactic radio source increases, the polarized radio emission is more influenced by the Faraday rotation effect in the metagalactic space. The magnetic field direction is determined and it is checked by statistical test.

Measurements of the Faraday rotation of polarized radio emission yield only products of the electron density and magnetic field strength in medium between the source and observer (see Eq. (1·1)). We attempt to determine separately an upper limit on the field strength or a lower limit on the thermal electron density in §3, on the basis of other data on the diffuse X-rays and the background non-thermal radio emissions. We shall suppose there that relativistic electrons kick the 2.7°K cosmical black-body photon up to the X-ray frequency region, and that the same electrons would gyrate simultaneously in the metagalactic magnetic field and emit synchrotron radiation, responsible for the diffuse non-thermal radio component.

It is also shown that the presence of a uniform metagalactic magnetic field contributes substantially to discussions on consmological problems on antimatter in the space up to a distance of $z \approx 2$.

Formations of galaxies in the expanding universe are discussed in Chapters I and IV in the present Supplement, suggesting that gaseous proto-galaxies may be generated by thermal instabilities (including turbulence effect) in the background gas at cosmic age $10^{6 \sim 7}$ years. The initial diameter of the proto-galaxy is already of the same magnitude as the present galaxy, and the magnetic field at this epoch is estimated as $10^{-5 \sim -6}$ gauss from the expansion ratio of the universe and the present strength of the metagalactic magnetic field. These coincidences to the present values could not be regarded as merely accidental, but they suggest an origin of galactic magnetic fields

the frozen-in of metagalactic magnetic fields to the condensing proto-galaxy. However, the magnetic field configurations in the Galaxy and in external galaxies such as in the Large and the Small Magellanic Clouds cannot be accounted for only in terms of the frozen-in of metagalactic magnetic fields to galaxies, but they must be explained by magneto-hydrodynamics at a level of the galaxy.

It is widely accepted that magnetic lines of force are frozen in inter-stellar gas, and the gas in the Galaxy is in differential rotation. Therefore, the helical magnetic field discussed in §1 cannot be in a stationary state but it is sheared very rapidly to lose its identity in 10^8 years near the sun. In §4 of the present paper, we intend to overcome this difficulty and to find magneto-hydrodynamical conditions that the helical magnetic field can be maintained in a stationary state (Fujimoto and Miyamoto 1969, 1970). It is shown that the helical field in the spiral arm is dynamically permissible, only if the interstellar gas rolls around the arm axis, superimposed on galactic rotation. On the basis of the λ21-cm line survey of galactic plane by Wester-hout (1966, 1969), we search for rolling motions of hydrogen gas around the arm axis. In §5 we make extensive distribution diagrams of the rolling motion along the various arms and discuss the possible formation of helical magnetic fields.

Prendergast (1963), Fujimoto (1963) and Freeman (1965) have investi-gated dynamics of gas in the barred galaxy and predicted that interstellar gas performs a large-scale and high-velocity circulation in the bar. deVaucou-leurs and deVaucouleurs (1963) have first observed the high-velocity gas streaming in the barred galaxy NGC 4631. Thus we expect that magnetic field topology in the bar is drastically different from the one in the Galaxy. Indeed, as mentioned earlier, the magnetic field distribution in the LMC determined by Visvanathan (1966), Mathewson and Ford (1970) and Schmidt (1970) suggest this tendency. In the final section of the present paper, we discuss motion of gas in the barred galaxy from a magneto-hydrodynamical point of view, and attempt to find a possible magnetic field configuration in the bar, so that it may serve to understand the field structures so far observed and the ones that will be observed in more detail in future.

§2. Search for metagalactic magnetic field by Faraday rotation of emissions from extragalactic radio sources

2-1 *Sources of data*

In earlier investigations on Faraday rotations in metagalactic space (Sofue, Fujimoto and Kawabata 1969; Kawabata, Fujimoto, Sofue and Fukui 1969), we have used the data of the rotation measures determined by Berge and Seielstad (1967). After that, Gardner, Morris and Whiteoak (1969) have

published a more extended list of radio sources with rotation measures determined from polarization measurements between $\lambda = 11$ cm and 21 cm.

The rotation measures of Berge and Seielstad (1967) are in good agreement with those by Gardner, Morris and Whiteoak (1969) for all listed in both tables but 3C 175 and we use the data by the latter for the present statistics. For 3C 175, Berge and Seielstad have obtained a rotation measure of 192 rad m^{-2}, while Gardner, Morris and Whiteoak have obtained 15 rad m^{-2}. This radio source has a galactic latitude of 10° and does not affect our arguments on metagalactic components of Faraday rotations, because we use only radio sources at $|b| > 35°$ in most of our following arguments.

In the list of rotation measures by Gardner, Morris and Whiteoak (1969), rotation measures for some radio sources are determined by using polarization angle at only two wavelengths. In such cases, we have checked their validity by use of the polarization measurement at $\lambda = 6$ cm of Gardner, Whiteoak and Morris (1969) and have justified most of them. For the radio source PKS 1123-35, Gardner, Morris and Whiteoak (1969) have chosen a value of -8 rad m^{-2}, but a value of -107 rad m^{-2} is in better agreement with $\lambda = 6$ cm obsevations.

From the list of radio sources of known rotation measures by Berge and Seielstad (1967) and Gardner, Morris and Whiteoak (1969), we select eighty six sources of known redshifts and twelve sources identified with normal or radio galaxies brighter than 17 magnitude. Table I gives the magnitudes of redshit as well as the values of rotation measure for these ninety eight sources.

2-2   *Dependence of rotaion measures on galactic coordinates and redshifts*

The ninety eight radio sources listed in Table I are divided into three classes according to the magnitudes of their redshifts; class 1 for the sources with $z \leq 0.1$, class 2 for those with $0.1 < z < 0.5$ and class 3 for those with $z \geq 0.5$. Radio sources identified with galaxies brighter than 17 magnitude are added to class 1 sources. Incidentally, all of class 1 and class 3 radio sources are galaxies and quasi-stellar radio sources, respectively.

For each class, absolute values of rotation measure are plotted against the galactic latitude in Fig. 1. Scatters in the rotation measures both for class 3 (O) and for class 1+2 (●) are very large at $|b| < 35°$, and then there is no doubt that the distribution of rotation measures is mainly due to galactic Faraday rotations. Beyond $|b| = 35°$, scatters in the rotation measure are small for class 1 and class 2 sources. Fifteen sources out of twenty in class 1 have rotation measures less than 15 rad m^{-2}, and all but PKS 2152-69 in the remaining five sources have rotation measures around 20 rad m^{-2}. Only one source, PKS 2152-69, has a rotation measure of 34 rad m^{-2}. On the other hand, most of radio sources with $z > 0.5$ have rotation measures exceeding 15 rad m^{-2} even at $|b| > 35°$. It is to be noted that

M. Fujimoto, K. Kawabata and Y.•Sofue

Table I.   Rotation measures and redshifts of radio sources.

PKS No.	Other designation	l	b	R.M.	z	References to $z^{a)}$	Notes
0017+15	3C 9	112	−47	−25	2. 012	1	Q.S.O.
0034−01	3C 15	115	−64	−13	0. 0733	2	
0035−02	3C 17	115	−65	+ 1	0. 2201	3	
0055−01	3C 29	126	−64	+ 2	0. 0450	4	
0056−00	PHL 923	127	−63	− 1	0. 72	5	Q.S.O.
0106+01		132	−61	−16	2. 107	1	Q.S.O.
0106+13	3C 33	129	−49	−11	0. 0600	6	
0131−36	01−311	262	−77	+ 5	0. 0297	5	
0133+20	3C 47	136	−41	−17	0. 425	1	Q.S.O.
	3C 48	134	−29	−53	0. 367	7	Q.S.O.
0159−11	3C 57	173	−67	+ 4	0. 669	1	Q.S.O.
0237−23		207	−65	+18	2. 223	1	Q.S.O.
0300+16	3C 76.1	163	−36	−17	0. 0326	2	
0305+03	3C 78	175	−45	+12	0. 0289	6	NGC 1218
0307+16	3C 79	164	−34	−15	0. 2561	3	
0319−37	For A(a)	240	−57	− 2. 8	0. 0058	8	
0322−37	For A(b)	240	−57	− 3. 5	0. 0058	8	
	3C 84	151	−13	+55	0. 0199	9	
0325+02	3C 88	181	−42	+21	0. 0302	6	
0336−01	CTA 26	188	−42	+23	0. 852	10	Q.S.O.
0350−07	3C 94	197	−43	+23	0. 962	1	Q.S.O.
0356+10	3C 98	180	−31	+82	0. 0306	6	
0403−13		206	−43	+ 4	0. 571	1	Q.S.O.
0410+11		182	−28	−12	0. 3056	2	
0430+05	3C 120	190	−27	+ 8	0. 0333	2	Seyfert
0511+00	3C 135	200	−21	+47	0. 1270	11	
0518+16	3C 138	187	−11	0	0. 754	1	Q.S.O.
0518−45	Pic A	252	−35	+47	0. 0342	6	
0521−36	05−36	241	−33	+ 6	0. 061	5	
0618−37	06−37	245	−22	+ 1			16. 6 mag. dB
0634−20	06−210	230	−12	+41			16. 8 mag. E
	3C 171	162	+22	+59	0. 2387	6	
0710+11	3C 175	205	+10	+15	0. 768	1	Q.S.O.
0736+01		217	+11	+27	0. 191	1	Q.S.O.
0802+24	3C 192	197	+27	+23	0. 0599	7	
0806−10	3C 195	231	+12	−31	0. 107	8	
0838+13	3C 207	213	+30	+22	0. 684	1	Q.S.O.
0843−33	08−38	256	+ 6	+68			⌠NGC 2663 ⌡12. 3 mag. E3
0859−14		242	+21	+ 8	1. 327	1	Q.S.O.
	3C 219	174	+45	−10	0. 1745	6	CD 5

Continued Table I

PKS No.	Other designation	l	b	R.M.	z	References to z[a]	Notes
0945+07	3C 227	229	+42	− 7	0. 0855	4	
1040+12	3C 245	233	+56	+31	1. 029	1	Q.S.O.
	3C 254	173	+66	−23	0. 734	12	Q.S.O.
1116+12	4C 12. 39	242	+64	− 7	2. 118	1	Q.S.O.
1123−35	11−33	284	+24	−107[b]			16. 0 mag. E3
1127−14		275	+44	+31	1. 187	1	Q.S.O.
1136−13	11−18	278	+45	−22	0. 554	1	Q.S.O.
1148−00		273	+59	0	1. 982	1	Q.S.O.
1216+06	3C 270	282	+67	+10	0. 00697	10	NGC 4261
1222+13	3C 272. 1	278	+74	− 5	0. 00293	10	M 84
1226+02	3C 273	290	+64	+ 1	0. 158	1	Q.S.O.
1241+16	3C 275. 1	293	+79	−18	0. 557	1	Q.S.O.
1252−12	3C 278	304	+50	−12	0. 0143	8	
1253−05	3C 279	305	+57	+24	0. 538	1	Q.S.O.
1322−428 1322−427	Cen A	310	+19	−60	0. 0019	13	NGC 5128
1328+254	3C 287	23	+81	−67	1. 055	1	Q.S.O.
	3C 286	57	+81	+ 4	0. 846	12	Q.S.O.
1330+02	3C 287. 1	326	+63	+ 2	0. 2156	12	
1332−33 1333−33 1334−33	13−33	313	+28	−32	0. 0114	10	
1335−06	13−011	323	+55	−13	0. 625	1	
1354+19		9	+73	+ 7	0. 720	1	Q.S.O.
1414+11	3C 296	358	+64	− 3	0. 0237	12	NGC 5532
1502+26	3C 310	39	+60	+14	0. 0543	6	
1510−08	15−06	351	+40	−10	0. 361	1	Q.S.O.
1511+26	3C 315	39	+58	0	0. 1086	5	
1514−24		341	+28	−20			16. 2 mag. E
1545+21	3C 323. 1	32	+49	+20	0. 264	1	Q.S.O.
1559+02	3C 327	12	+38	+12	0. 1041	6	
1610−608		325	− 7	−72			12. 8 mag. E3
1622+23	3C 336	40	+42	+31	0. 927	1	Q.S.O.
1637−77		314	−20	+50			16 mag. D3
	3C 345	63	+41	+19	0. 5940	12	Q.S.O.
1648+05	3C 348	23	+29	+11	0. 157	8	Her A
1717−00	3C 353	23	+21	+36	0. 0307	6	
	3C 380	77	+24	+31	0. 691	12	Q.S.O.
1836+17	3C 386	47	+11	+69	0. 0033	5	
1949+02	3C 403	42	−12	−39			16. 5 mag. S0
1954−55		343	−31	−17			16. 5 mag. E
2040−26	20−212	19	−35	−21			15. 4 mag. E
2104−25	21−21	21	−40	−11			16. 8 mag. E

Continued Table I

PKS No.	Other designation	l	b	R.M.	z	References to z[a]	Notes
2115−30	21−34	16	−43	+28	0.98	10	Q.S.O.
	3C 430	100	+ 8	−162	0.0167	8	
2121+24	3C 433	74	−18	−76	0.1025	3	
2135−14	21−115	38	43	+19	0.200	1	Q.S.O.
2152−69	21−64	321	−41	+34	0.0266	5	
2209+08		69	−38	−28	0.486	10	Q.S.O.
2212+13	3C 442	75	−34	−38	0.0270	10	NGC 7236,7
2221−02	3C 445	62	−47	+ 5	0.0568	6	
2223−05	3C 446	59	−49	−21	1.406	1	Q.S.O.
2230+11	CTA 102	77	−39	−47	1.037	1	Q.S.O.
2247+11		81	−41	−19	0.0268	10	
	3C 452	98	−17	−272	0.0820	6	
2249+18	3C 454	88	−36	−87	1.757	1	Q.S.O.
2251+15	3C 454.3	86	−38	−52	0.859	1	Q.S.O.
2252+12		84	−41	+13	0.0334	4	
2309+09	3C 456	86	−46	+ 3	0.2337	6	
2313+03	3C 459	83	−51	+ 7	0.2205	6	
2356−61	23−64	314	−55	+23			16 mag. D

a) References to z: 1 Burbidge (1967a), 2 Burbidge (1967b), 3 Bolton and Ekers (1966), 4 Sandage (1967), 5 Gardner, Morris and Whiteoak (1969), 6 Schmidt (1965), 7 Schmidt and Matthews (1964), 8 Matthews, Morgan and Schmidt (1964), 9 Humason, Mayall and Sandage (1956), 10 Gardner, Whiteoak and Morris (1969), 11 Bolton and Kinman (1966), 12 Sandage (1966), 13 Evans (1967).

b) Gardner, Morris and Whiteoak (1969) have cited a value of -8 rad m^{-2}, the smallest value reduced from observations at two wave lengths. This value of rotation measure disagrees with 6 cm observation. Then we determined the rotation measure by using observations by Gardner, Morris and Whiteoak (1969) and Gardner, Whiteoak and Morris (1969).
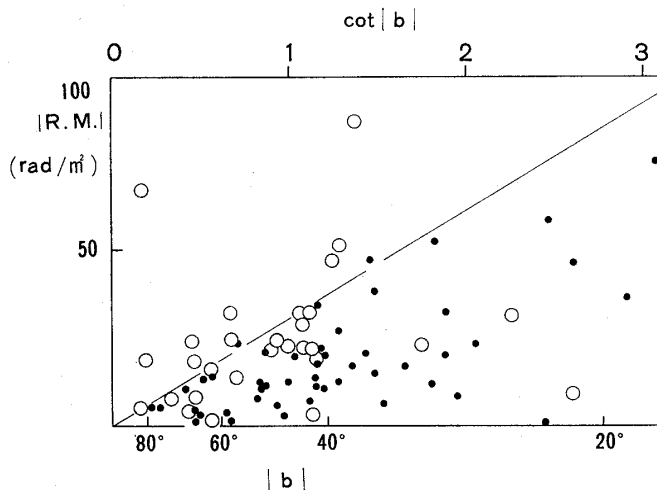

Fig. 1. Latitude dependence of the absolute magnitudes of rotation measures for radio sources with $z \geq 0.5$ (O) and those with $z \leq 0.5$ (●). Note that the open circles are more scattered vertically compared with the dark ones; the dark circles are distributed below a line of $|R.M.| = 30 \times \cot|b|$ rad m^{-2}.

one source 3C 287 ($z=1.055$) at $b=81°$ has a rotation measure of -67 rad m^{-2} and another source 3C 454 ($z=1.757$) has a rotation measure of -87 rad m^{-2}, the largest at $|b|>35°$.

Standard deviations of rotation measures at $|b|>35°$ are 13.9, 13.1 and 30.5 rad m^{-2} for class 1, 2 and 3 sources, respectively. The standard deviations for class 1 and 2 sources at $|b|>35°$ have almost the same values, but the standard deviation for class 3 sources is much larger than those for class 1 and 2. Such a discrepancy between class 1 and 3 sources can be expected by chance only with a probability less than 1 percent.

From these facts, the following discussions are concerned mostly with radio sources at $|b|>35°$, where the metagalactic Faraday rotation is not so much disturbed by a magnetized plasma in the Galaxy. In Fig. 2, we have plotted absolute values of rotation measure against redshifts for radio sources at $|b|>35°$. An increase in scatter of rotation measures with z can be seen more clearly in this figure, indicating that a large portion of the Faraday rotation takes place in the intergalactic space for radio sources at $|b|>35°$.
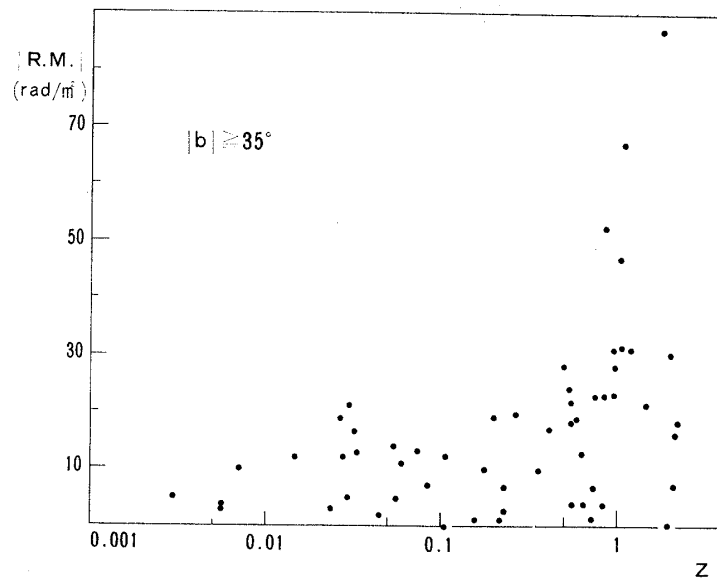

Fig. 2. Redshift dependence of the magnitudes of rotation measures for radio sources at $|b|\geqq35°$. The scatter of rotation measures increases with the redshift.

Now we build a distribution map of rotation measures for class 1 and 3 sources in Fig. 3, where we use only sources at $|b|>35°$ for class 3. From the above discussions, we can consider the distribution map for class 1 represents the Galactic Faraday rotations. As is already mentioned by Morris and Berge (1964), Gardner and Davies (1966), Berge and Seielstad (1967), and Gardner, Morris and Whiteoak (1967), rotation measures due to the galactic magnetic field have negative values in a tilted belt from $l\sim100°$,
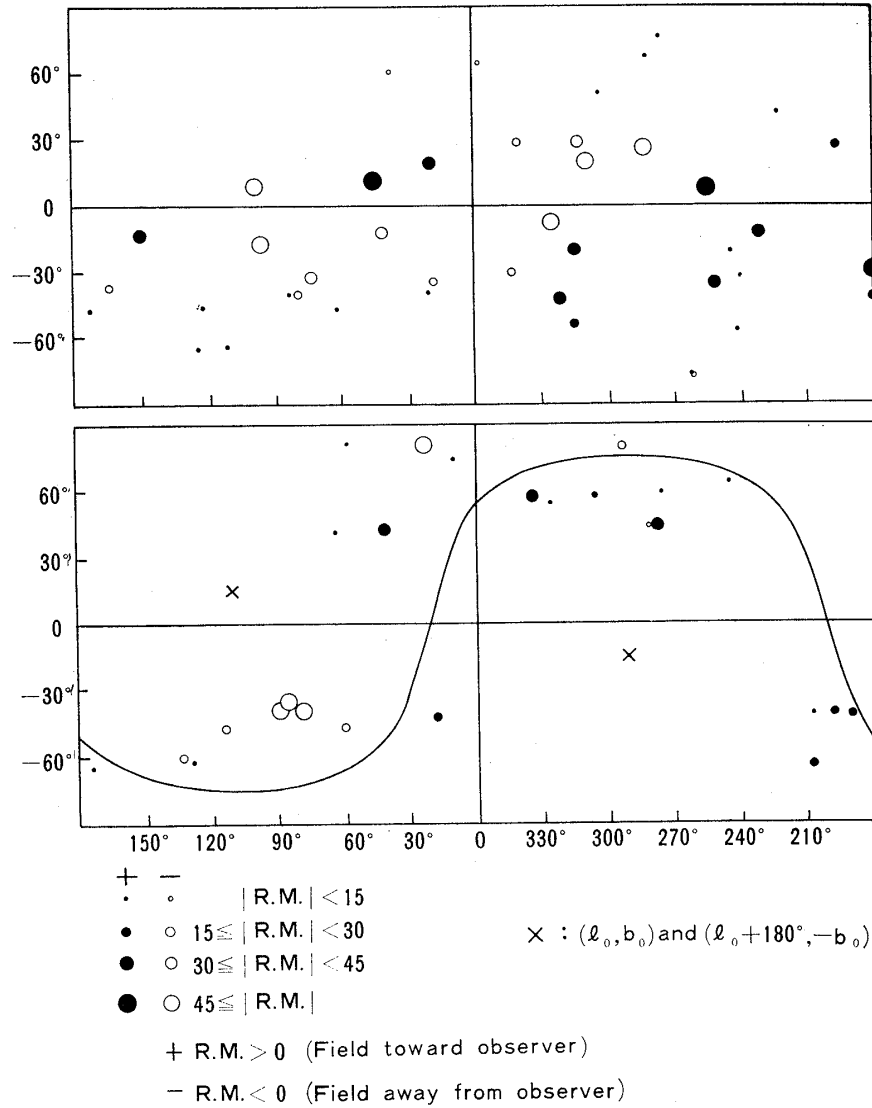
Fig. 3. Distributions of the rotation measure in galactic coordinates for radio sources
with $z \leq 0.1$ (upper diagram), and for those with $z \geq 0.5$ at $|b| \geq 35°$ (lower diagram).
In the upper diagram the rotation measures are negative in the tilted belt from the
lower left quadrant to the upper right quadrant, positive in the other part of the sky,
and they are very small at $|b| \geq 35°$. In the lower diagram a great circle of the
sky is given with a pole at $l_0 = 110°$, $b_0 = 15°$. Most of radio sources in north of
this line have negative rotation measures, whereas those in south of this line have
positive rotation measures.

$b < 0$ through $l \sim 270°$, $b > 0$, and have positive values from $l \sim 270°$, $b < 0$
through $l \sim 100°$, $b > 0$.

Sofue, Fujimoto and Kawabata (1969) have pointed out different distri-
butions of rotation measures between radio sources with large redshifts and
those with small redshifts in the regions at $l \sim 100°$, $b \sim -30°$ and $l \sim 280°$,
$b \sim 30°$. They have claimed that the rotation measures in the region $l \sim 100°$,
$b \sim -30°$ have small positive values for the radio sources with $z < 0.1$ and
they have large negative values for those with $z > 0.1$, and that the opposite

holds in the region $l\sim280°$, $b\sim+30°$. From this result, they have inferred that a large-scale metagalactic magnetic field runs from $l\sim280°$, $b\sim30°$ through $l\sim100°$, $b\sim-30°$.

This argument is not exactly correct in view of the distribution map of rotation measures constructed from the increased data, but we can still find such a tendency in the distribution maps of rotation measures for class 1 and 3 sources. In §2-3 of this chapter, the direction of the uniform metagalactic magnetic field is determined to be $l\sim110°$, $b\sim15°$. A line in Fig. 3 for class 3 represents the plane perpendicular to the direction of the uniform metagalactic magnetic field. By dividing the sky into two parts by this line, one finds that most of distant radio sources in the northern hemisphere have negative rotation measures and most of those in the southern hemisphere have positive rotation measures. A small restricted region of the sky $l=69°\sim87°$, $b=-34°\sim-51°$ contains a relatively large number of radio suorces of known rotation measures and redshifts, and is suitable for investigating a dependence of rotation measures on redshifts. In this region, radio sources with small redshifts have small negative rotation measures, and those with large redshifts have large negative rotation measures (see Fig. 3). In Fig. 4, we plot rotation measures against redshifts for the sources in this region. A radio source 3C 442 has the lowest galactic latitude and its rotation measure is probably affected by galactic Faraday rotation. It is clearly seen that rotation measures increase (negatively) with z.

In the remaining part of the sky, there is no region so populated with radio sources of known rotation measures and redshifts, and so we cannot construct a diagram like Fig. 4 for other parts of the sky. However, we may point out several discrepanices between sources in the two
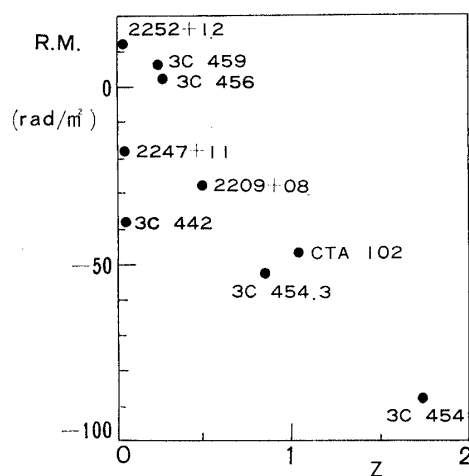

Fig. 4. Dependence of rotation measures on redshifts for radio sources in narrow region about $l=80°$, $b=-40°$. A good correlation is found between R.M. and z.

maps of Fig. 3. In a region around $l=16°\sim21°$, $b=35°\sim43°$, we have two radio sources identified with galaxies brighter than 17 magnitude and one quasi-stellar radio source with $z=0.98$. The two radio sources identified with bright galaxies have small negative rotation measures and the quasi-stellar radio source has a positive rotation measure. In other words, a reversal of the sign of rotation measure occurs between class 1 and 3 sources.

In a region $l=270°\sim340°$, $b=40°\sim60°$, we have three pairs of radio sources located within about 10° in separation. PKS 1136-13 ($z=0.554$) located

at $l=278°$, $b=+45°$ has rotation measure of -22 rad m^{-2} and PKS 1127-14 ($z=1.187$) located at $l=275°$, $b=+44°$ has rotation measure of $+31$ rad m^{-2}. 3C 278 ($z=0.0143$) at $l=304°$, $b=+50°$ has rotation measure of -12 rad m^{-2}, and 3C 279 ($z=0.540$) at $l=305°$, $b=+57°$ has rotation measure of $+24$ rad m^{-2}. 1335-06 ($z=0.625$) at $l=323°$, $b=+55°$ has rotation measure of -13 rad m^{-2} and 3C 245 ($z=1.029$) at $l=233°$, $b=+56°$ has rotation measure of $+31$ rad m^{-2}. Although it is difficult to estimate galactic components of Faraday rotations in this region, there is a tendency for the rotation measure to increase towards large positive values with z in all of these three pairs of radio sources.

2-3   Uniform component of the metagalactic magnetic field

Let us suppose that the redshift z of a radio source is proportional to its distance and the Faraday rotation takes place in the metagalactic space containing a uniform magnetic field and thermal electrons of uniform density. If this is the case, the rotation measure should be proportional to $z \cdot \cos\theta$, where θ denotes the angle between the direction of the source and that of the uniform metagalactic magnetic field.

As shown in §2-2, the dependence of the rotation measure on the redshift can be found only at intermediate and higher galactic latitudes. Therefore, sixty one radio sources at latitudes higher than 35° are selected out of the ninety eight radio sources listed in Table I, and are used for statistics in the present section.

We compute the correlation coefficients between the rotation measures and $z \cdot \cos\theta$ for various presumed directions of the metagalactic magnetic field (l_0, b_0) over the sky. The maximum correlation coefficient of 0.573 is obtained when we take the direction (110°, 15°). The plot of R.M. against $z \cdot \cos\theta$ for this presumed direction of the metagalactic magnetic field is shown in Fig. 5, where one finds graphically a good correlation between them. A similar investigation has been made previously by Kawabata, Fujimoto, Sofue and Fukui (1969) by using thirty five radio sources. They have found a maximum correlation coefficient of 0.61 for (115°, $-5°$). The newly determined direction of the metagalactic magnetic field is close to the previously determined one, and the maximum correlation coefficient remains unchanged. Reinhardt and Thiel (1970) and Reinhardt (1971a) have made similar investigations to the present paper, and have found almost the same direction of the metagalactic magnetic field $l_0=110°$, $b_0=+10°$, by using radio sources beyond $b=\pm30°$, instead of $\pm35°$.

When we take $l_0=115°$ and $b_0=-15°$ as the direction of the metagalactic field, the present data lead to the correlation coefficient as low as 0.454. By this reason Brecher and Blumenthal (1970) questioned the correlation between R.M. and $z \cdot \cos\theta$. However, a correlation coefficient larger than 0.411 in sixty one data can be expected by chance with a proba-
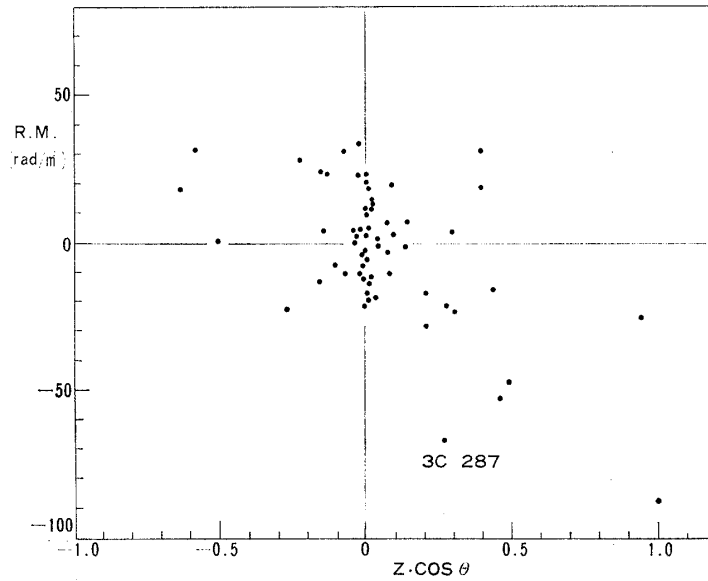
Fig. 5. Correlation between rotation measures and $z \cdot \cos\theta$ for radio sources of $|b| \geqq 35°$. The direction of the uniform metagalactic magnetic field is taken as $l_0 = 115°$, $b_0 = 15°$, in which the correlation coefficient attains its maximum value of 0.573, and θ is the angle between the direction of source and (l_0, b_0).

bility of only 0.1 percent from null correlation ensemble, and then we consider that the correlation between R.M. and $z \cdot \cos\theta$ is significant, even if the correlation coefficient is 0.454.

In Fig. 6, the rotation measures are plotted against $|\cos\theta|$, where signs of the rotation measures are reversed for radio sources with negative value of $\cos\theta$. A large correlation can be expected also in this diagram if the Faraday rotation takes place in the Galaxy and the local magnetic field is directed towards (l_0, b_0). No noticeable correlation can be found between $\pm$R.M. and $|\cos\theta|$, and then the correlation in Fig. 5 cannot be attributed to the local magnetic field in the Galaxy.

Thus, the correlation between the rotation measure and $z \cdot \cos\theta$ implies, in the cosmological hypothesis on quasi-stellar radio sources, a
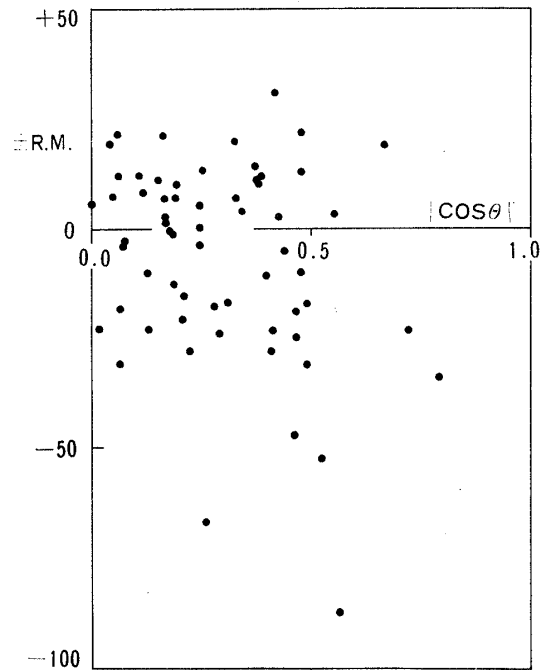

Fig. 6. Correlation between the rotation measures and $|\cos\theta|$ for radio sources of $|b| \geqq 35°$ is given, in order to show the correlation in Fig. 5 is significant. For radio sources of $\cos\theta < 0$, the signs of R.M. are reversed in this figure. One finds only a weak correlation between $\pm$R.M. and $|\cos\theta|$.

contribution of the uniform component of the metagalactic magnetic field to the Faraday rotation of emissions from linearly polarized radio sources. The largest value of the redshift for the sources used in the present investigation is 2.223, and then the large-scale metagalactic magnetic field is approximately uniform at least up to a distance of this order of z.

All of the earlier investigators have left a radio source 3C 287 from their statistics, because it has an exceptionally large rotation measure compared with other radio sources at high galactic latitudes. This radio source had destroyed all correlations found before and had weakened all the earlier discussions. However, this radio source 3C 287 has a large redshift $z=1.055$ and is now located at a rather right place in the (R.M. $-z \cdot \cos\theta$)-plane in Fig. 5; the large rotation measure of this source can be regarded as due to the uniform metagalactic magnetic field.

When we subtract the contribution of the metagalactic magnetic field from the observed rotation measures in Table I, we can build a distribution map of net rotation measures in the Galaxy (Fig. 7). Comparing Fig. 7 with the distributions of rotation measures of Gardner and Davies (1966), Berge and Seielstad (1967) and Gardner, Whiteoak and Morris (1967), we find that the anomalous region of the negative rotation measures near $l=75°$, $b=-40°$ vanishes in Fig. 7. However, no other drastic change is found between them, and the original features of a large-scale order imposed on the distribution of rotation measures in galactic coordinates are still valid.
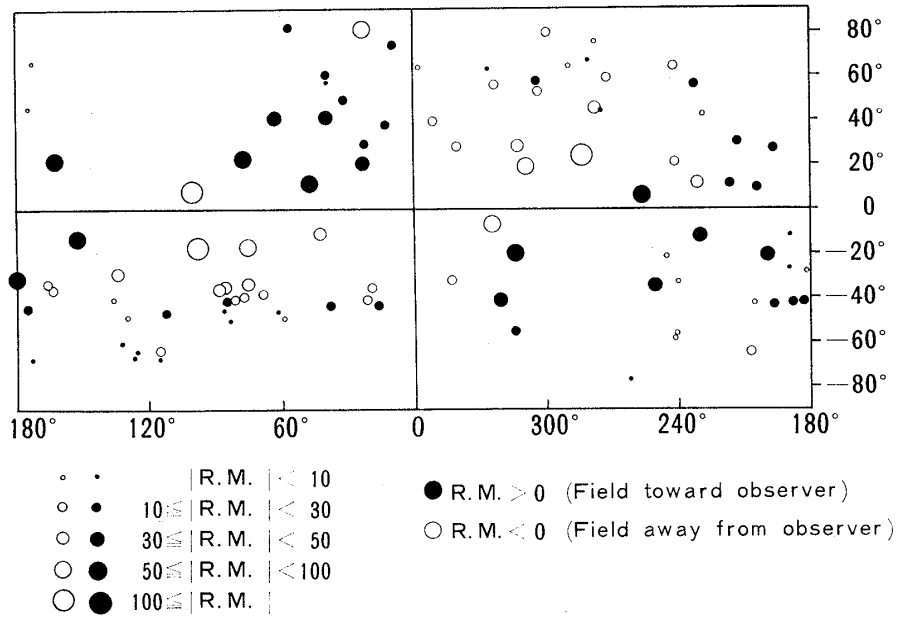

Fig. 7. Distribution of rotation measures of the galactic Faraday rotation for radio sources with known redshift. Contributions from the metagalactic magnetic field R.M. $=-48.3$ $z \cdot \cos\theta$ rad m^{-2} are subtracted from the observed rotation measures listed in Table I. We have taken $l_0=110°$, $b_0=15°$.

Since the rotation measure represents a quantity $N_e B_{//}$ integrated over the space between source and observer, the present results do not rule out the existence of superimposed irregular component of the magnetic field. Indeed, the scatters in the correlation diagram in Fig. 5 may be due to irregular distributions of B and N_e or of both. Note that the scatters may be attributed also to the Faraday rotation in the Galaxy and radio sources and to errors in determining rotation measures.

We divide sixty one radio sources of $|b| > 35°$ into five groups according to the magnitude of z and plot variance of $(O-C)^2$ for each group in Fig. 8. Standard deviation of $(O-C)$ is about 14 rad m^{-2} for radio sources in the first two groups of $z < 0.4$, and therefore an upper limit on the galactic Faraday rotations for radio sources at $|b| > 35°$ can be put 14 rad m^{-2}. Average value of $(O-C)^2$ for each group of $z > 0.4$ have a tendency to increase with z. At present, we cannot specify the cause of

Fig. 8. Dependence of $\Sigma(O-C)^2/N$ on redshift z. O and C represent observed values of R.M. and those calculated from the correlation in Fig. 5, respectively; R.M. $= -48.3$ $z\cdot\cos\theta$ rad m^{-2}.

the monotonic increase of average values of $(O-C)^2$ with z, but in any way, we can put an upper limit on the fluctuations in B and N_e as $\overline{\{\varDelta(N_e B)\}^2}^{1/2}$ $= 10^{-14}/\sqrt{s}$, where

$$s = \text{(fluctuation wave length)} \times H/c,$$

with $H = 100$ km sec^{-1} Mpc^{-1}, the Hubble constant and c, the light velocity.

§3. Magnetic field and matters in metagalactic space

3-1 *Metagalactic magnetic field strength*

In the cosmological hypothesis on quasi-stellar radio sources, the correlation between rotation measures and $z\cdot\cos\theta$ implies a contribution of the uniform component of the metagalactic magnetic field to the Faraday rotation of emissions from linearly polarized radio sources. From the correlation diagram in Fig. 5, we obtain the relation

$$N_e B = 2 \times 10^{-14} \text{ gauss cm}^{-3}, \tag{3·1}$$

where N_e denotes the thermal electron density and B the field strength in the metagalactic space, and we have taken the Hubble constant $H = 100$ km sec^{-1} Mpc^{-1}. When $N_e = 10^{-5}$ cm^{-3}, the field strength is 2×10^{-9} gauss.

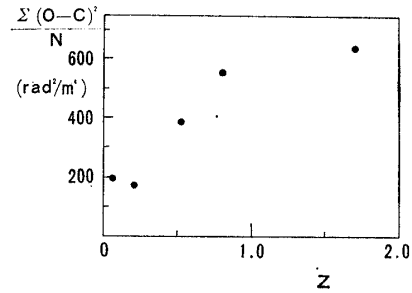Since measurements of the Faraday rotation yield only the product of electron density and magnetic field strength in medium between source and observer, another clue is required for unique determination of the field strength and the electron density. It has been discussed by Felten and Morrison (1966) that the observed diffuse component of X-rays is of the cosmic origin as the inverse Compton radiation from relativistic electrons in the cosmic black-body radiation at $2.7°K$. If this is the case, the same relativistic electrons gyrate around the metagalactic magnetic field and emit synchrotron radiations. Therefore, we can obtain another information on the metagalactic magnetic field by combining the observed X-ray background radiations and the radio background radiations in non-thermal component.

Let the radius of the universe at cosmic age t be denoted by R, then the density of the relativistic electrons in a region of the metagalactic space may be taken to have a power-law form given by

$$n(\gamma)d\gamma = K(t_0/t)^\beta (R_0/R)^3 \gamma^{-\alpha} d\gamma,$$

with

$$\gamma = E/(mc^2),$$

where subscripts 0 are for the quantities at the present cosmic age t_0, m denotes the electron mass and other symbols have their usual meanings. In the above expression, $(t_0/t)^\beta$ represents evolutionary effects of relativistic electron sources with still unspecified parameter, and $(R_0/R)^3$ a dilution of relativistic electrons due to expansion of the universe.

The relativistic electron kicks low energy photons of the cosmic black-body radiation up to the X-ray frequency region. The resultant volume emissivity of the X-rays is given by

$$\left(\frac{dP}{d\nu dt}\right)_c = \frac{2}{3}\sigma_T c\left(\frac{h}{3.6k}\right)^{(3-\alpha)/2} \rho_R T^{(\alpha-3)/2} \nu^{(1-\alpha)/2} K\left(\frac{t_0}{t}\right)^\beta \left(\frac{R_0}{R}\right)^3, \qquad (3\cdot2)$$

with

$$\rho_R = \frac{4\sigma}{c} T^4,$$

where k represents the Boltzmann constant, and σ and σ_T the Stefan-Boltzmann constant and the Thomson cross-section, respectively. In the expanding universe, the temperature T of the cosmic black-body radiation can be expressed by

$$T = T_0(R_0/R),$$

using the present temperature of the cosmic black-body radiation, $T_0 = 2.7°K$.

The volume emissivity of synchrotron radiation due to the same relativistic electrons in the metagalactic magnetic field B is given by

$$\left(\frac{dP}{d\nu dt}\right)_s = \frac{0.1}{\pi}\sigma_T c\left(\frac{4\pi mc}{3e}\right)^{(3-\alpha)/2} B^{(1+\alpha)/2}\nu^{(1-\alpha)/2}K\left(\frac{t_0}{t}\right)^\beta\left(\frac{R_0}{R}\right)^3, \quad (3\cdot3)$$

where magnetic field strength is assumed to vary as $B_0(R_0/R)^2$ in the expanding universe.

From Eqs. (3·2) and (3·3), and by making use of the Robertson-Walker metric,

$$ds^2 = dt^2 - \frac{R^2(t)}{c^2}\frac{1}{\left(1+\frac{k}{4}r^2\right)^2}\{dr^2 + r^2(d\theta^2 + \sin^2\theta d\varphi^2)\}, \quad (3\cdot4)$$

one obtains the fluxes of the background radiation at the earth in the X-ray and radio frequency regions, ν_X and ν_R, as

$$j_X(\nu_X) = J_X\nu_X^{(1-\alpha)/2}\int_{t_e}^{t_0}\left(\frac{t_0}{t}\right)^\beta\left(\frac{R_0}{R}\right)^3 dt$$

and

$$j_R(\nu_R) = J_R\nu_R^{(1-\alpha)/2}\int_{t_e}^{t_0}\left(\frac{t_0}{t}\right)^\beta\left(\frac{R_0}{R}\right)^{(3+\alpha)/2} dt.$$

Here, the constants J_X and J_R are given by

$$J_X = \frac{2}{3}\frac{c}{4\pi}K\sigma_T\sigma\left(\frac{h}{3.6kT_0}\right)^{(3-\alpha)/2}\rho_{R0}$$

and

$$J_R = 0.1\frac{c}{4\pi}K\sigma_T\left(\frac{4\pi mc}{3e}\right)^{(3-\alpha)/2}B_0^{(1+\alpha)/2},$$

and t_e is the cosmic age after which the expanding universe is transparent for X-rays and non-thermal radio waves emitted by the relativistic electron.

Taking the ratio of j_R and j_X, we obtain

$$\frac{j_X}{j_R} = \frac{J_X}{J_R}\xi(\alpha, \beta)\left(\frac{\nu_X}{\nu_R}\right)^{(1-\alpha)/2}, \quad (3\cdot5)$$

where

$$\xi(\alpha, \beta) = \int_{t_e}^{t_0}(t_e/t)^\beta (R_0/R)^3 dt \Big/ \int_{t_e}^{t_0}(t_0/t)^\beta (R_0/R)^{(3+\alpha)/2} dt.$$

Since we have a good approximate relation, $R(t) \propto t^{2/3}$, for various models of the expanding universe, $\xi(\alpha, \beta)$ is written as

$$\xi(\alpha, \beta) = \frac{\alpha+3\beta}{3(\beta+1)}\frac{(t_0/t_e)^{(1+\beta)}-1}{(t_0/t_e)^{(3+\alpha)/2}-1}.$$

Observations of the diffuse component of X-rays give $(1-\alpha)/2 = -0.8$ or $\alpha = 2.6$ (Bleeker, Burger, Deerenberg, Scheepmaker, Swanenburg, Tanaka, Hayakawa,

Makino and Ogawa 1968). The numerical values of t_0/t_e and β are to be determined by the opacity of the universe and the evolution of relativistic electron sources which are still in controversy. However, as is shown numerically in Table II, $\xi(2.6, \beta)$ is insensitive to these values. Therefore, it is not necessary to be so concerned about the exact value of t_e/t_0 and the evolutionary effect of relativistic electron sources. Thus, the ratio (3·5) becomes

Table II. Numerical values of $\xi(2.6, \beta)$ for various combinations of β and t_0/t_e.

β t_0/t_e	0	2
10	1. 2	1. 3
30	1. 4	1. 5

$$\frac{j_X}{j_R} = (9.3 \sim 11.6) \times 10^{-13} B_0^{-1.8} \left(\frac{\nu_X}{\nu_R} \right)^{-0.8}. \qquad (3\cdot6)$$

The X-rays intensity j_X in diffuse component has been observed by rockets to be 2.4×10^{-26} erg cm^{-2} sec^{-1} str^{-1} Hz^{-1}, for example, at $h\nu_X = 6$ KeV (Bleeker et al. 1968). The brightness temperature of background radio emissions at 178 MHz is 80°K in the direction of minimum temperature (Turtle and Baldwin 1962). Therefore, we can put an upper limit on the radio intensity at 178 MHz as 2×10^{-19} erg cm^{-2} sec^{-1} str^{-1} Hz^{-1} for the meta-galactic synchrotron radiation, corresponding to a brightness temparature of 20°K.

Then we can obtain from Eq. (3·6) an upper limit on the metagalactic magnetic field as small as 2×10^{-8} gauss. This upper limit and Eq. (3·1) give a lower limit on the thermal electron density $N_e \geq 10^{-6}$ cm^{-3}, or the mass density in the metagalactic space is larger than 1.7×10^{-30} gr cm^{-3}, being six times Oort's (1958) value of the smoothed density of visible matter in the universe, 3×10^{-31} gr cm^{-3}.

3-2 Cosmological problems related to the (R.M.$-z\cdot\cos\theta$) relation

A rough lower limit on growing time of magnetic fields in dynamo actions may be given by l/v, where l and v represent the characteristic size of the metagalactic magnetic field and the velocity of circulation responsible for the dynamo action, respectively. By taking $l\sim3000$ Mpc($z\sim1$) and $v\sim$ 1000 km/s, the growing time of the field becomes $>3 \times 10^{12}$ years, exceeding the life of the universe. Thus the scale of the metagalactic magnetic field discussed in the preceding section is too large to attribute it to dynamo actions in the metagalactic space.

A possible origin of the large-scale metagalactic magnetic field can be considered to be a primordial homogeneous magnetic field. Zel'dovich (1965), Doroshkevich (1965) and Thorne (1967) have shown that the concept of a primordial homogeneous magnetic field is compatible with uniform anisotropic

model of the expanding universe. Since the primordial magnetic field exists despite the absence of any electric current anywhere, it is a frozen-in field irrespective of the conductivity of the matter in the universe.

We have made various discussions on matter, radiation and uniform magnetic field in metagalactic space under the implicit assumption that the universe does not contain antimatter. Reinhardt (1971b) has first claimed a large lower limit on the size of the regions of matter and antimatter in the vanishing-baryon-number cosmology (Alfvèn 1965; Harrison 1967; Omnés 1969 and 1970; and see the references in a paper by Reinhardt for further detailed discussions on antimatter) from evidence of the linear relation between $z \cdot \cos\theta$ and R.M. in Figs. 4 and 5, and he has concluded that the baryon number in the space from $z = 0$ to $z = 0.8$ does not vanish, or antimatter must be present in the region beyond $z = 0.8$ in the vanishing-baryon-number cosmology. Indeed, the linear relation between $z \cdot \cos\theta$ and R.M. contributes to discussions on matter and antimatter in the universe; a polarized radio wave performs the Faraday rotation in an opposite sense in a plasma of antimatter to that in a plasma of matter when a magnetic field is homogeneous on cosmological scale.

If we relax the vanishing-baryon-number cosmology, however, Reinhardt's (1971b) conclusion does not rule out the possibility that the universe contains some fractional amount of antimatter. In what follows we attempt to find an upper limit on the amount of antimatter in the metagalactic space by making use of models for matter and antimatter distributions.

The linear relation between R.M. and $z \cdot \cos\theta$ in Figs. 4 and 5 represents the presence of uniform components of plasma and magnetic field, and scatters of the data about this linear relation $\overline{R.M.} \propto z$ (see Fig. 8) are considered as due to fluctuations in electron density and magnetic field in intergalactic space and also to intrinsic rotation measures of radio sources. By assuming no fluctuations and no intrinsic rotation measures, and by attributing the scatter of the data about $\overline{R.M.}$ solely to the isotropic and random distribution of antimatter regions, we can determine an upper limit on the amount of antimatter in intergalactic space. Figure 9 shows a model for mass distribution along a line-of-sight, where s denotes a correlation length of antimatter gas cloud.]If the matter
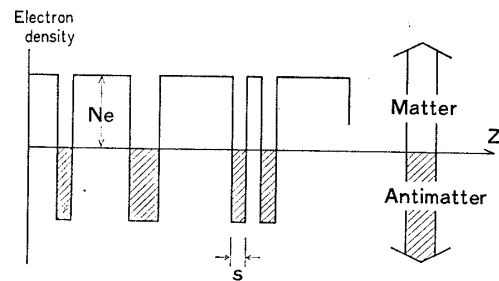

Fig. 9. A random distribution of antimatter clouds (shaded) along a line-of-sight. The positron number in a plasma of antimatter is taken as negative. The antimatter region is characterized by a correlation length s.

and antimatter occupy the space in the ratio $1-\alpha : \alpha$ along a line-of-sight, then the rotation measure of the radio source at z and with an angle θ with

respect to the direction (l_0, b_0) is

$$\text{R.M.} = \beta N_e B s \cos\theta \left[(1-\alpha)\frac{z}{s} - \alpha\frac{z}{s} \right]$$

$$= \beta N_e B (1-2\alpha) \cos\theta \cdot z, \tag{3·7}$$

where $\beta = 2.4 \times 10^{15}$ when the correlation length of the antimatter region is represented by sH/c with the Hubble constant, $H = 100$ km sec^{-1} Mpc^{-1}. Average of both sides of Eq. (3·7) over $z=0$ to $z=z$ yields

$$\overline{\text{R.M.}} = \beta N_e B (1-2\bar{\alpha}) \cos\theta \cdot z, \tag{3·8}$$

The linear relation between R.M. and $z \cdot \cos\theta$ is found in Eq. (3·8) and the observational results in Figs. 4 and 5 confirm $1-2\bar{\alpha} \neq 0$, or the metagalactic space up to $z \sim 2$ does not exactly satisfy the vanishing-baryon-number cosmology $(\bar{\alpha} = 0.5)$.

The dispersion about $\overline{\text{R.M.}}$ is given by Eqs. (3·7) and (3·8),

$$\sigma_{\text{R.M.}}^2 = \overline{(\text{R.M.} - \overline{\text{R.M.}})^2} = 4\beta^2 N_e^2 B^2 \cos^2\theta z^2 \overline{(\alpha - \bar{\alpha})^2}$$

$$= 4\beta^2 \bar{\alpha}^2 N_e^2 B^2 \cos^2\theta sz$$

or

$$\sigma_{\text{R.M.}} = 2\beta\bar{\alpha} N_e B \cos\theta \sqrt{sz}. \tag{3·9}$$

Equations (3·8) and (3·9) lead to the following ratio

$$\frac{\sigma_{\text{R.M.}}}{\overline{\text{R.M.}}} = \frac{2\bar{\alpha}}{1-2\bar{\alpha}} \sqrt{\frac{s}{z}}. \tag{3·10}$$

In Figs. 4, 5 and 8, one finds $\sigma_{\text{R.M.}}/\overline{\text{R.M.}} = 0.1 \sim 0.25$ at $z \approx 1$. Therefore, if the correlation length s is specified, Eq. (3·10) gives an upper limit on the amount of antimatter. We have calculated the ratio η for a variety of combinations of s and $(\sigma_{\text{R.M.}}/\overline{\text{R.M.}})$ evaluated at $z \sim 1$ (Table III), where

$$\eta = 1 - 2\bar{\alpha} = \frac{M_{\text{matter}} - M_{\text{antimatter}}}{M_{\text{matter}} + M_{\text{antimatter}}}.$$

The case $\eta \lesssim 0.03$ for $s \leq 10^{-5}$ concludes that Reinhardt's claim (1971b) to a large lower limit on the size of matter and antimatter regions is not always appropriate. Because the numerical value $\eta \lesssim 0.03$ is determined in a limited space of $z < 2$ and it may be regarded as mere fluctuations from the symmetric universe $(\eta = 0.0)$ with far larger space of $z > 2$. The magnitude of $s = 10^{-5}$ corresponds to 30 kpc, which seems, of course, too small for the typical size of the metagalactic clouds of matter and antimatter.

The numerical values in Eq. (3·1), $N_e B = 2 \times 10^{-14}$ gauss cm^{-3}, has been evaluated in the case of no antimatter, $\eta = 1$, but if antimatter is distributed like in the model in Fig. 9, the above value is modified as $N_e B = 2 \times 10^{-14} \eta^{-1}$ gauss cm^{-3}. On the basis of the background non-thermal radio emission and

the diffuse X-rays, we have imposed an upper limit on B, 2×10^{-8} gauss, and therefore, a lower limit on N_e, 10^{-6} electron cm^{-3}. Although upper limits on N_e are very uncertain at this moment, we may take them as $N_e = 4 \times 10^{-5}$ electron/cm^3; the electron number density in the intergalactic space of the Local Group (Tadokoro 1969). We have

$$B < 2 \times 10^{-8} \text{ gauss}$$

and

$$N_e < 4 \times 10^{-5} \text{ electron/cm}^3. \qquad (3 \cdot 11)$$

The factor η^{-1}, and thus $N_e B$ increase to infinity as η approaches zero $(M_{matter} \approx M_{antimatter})$, but the upper limit $(3 \cdot 11)$ imposes a constraint on η,

$$2 \times 10^{-14} \eta^{-1} < 8 \times 10^{-13}$$

or

$$\eta > 0.025.$$

If we take a value $N_e < 10^{-5}$ electron/cm^3, we have

$$\eta > 0.1.$$

Permitted combinations of s and $(\sigma_{R.M.}/\overline{R.M.})_{z \sim 1}$ to $\eta > 0.025$ and $\eta > 0.1$ are indicated by the solid lines in Table III.

Table III. The ratio η for various combinations of s and $\sigma_{R.M.}/\overline{R.M.}$

$s^{a)}$ \ $\sigma_{R.M.}/\overline{R.M.}$	0.1	0.25	0.5	
10^{-6}	0.01	0.004	0.002	
10^{-5} (30 kpc)	0.03	0.012	0.006	
10^{-4}	0.09	0.04	0.02	
10^{-3}	0.24	0.11	0.06	$N_e < 4 \times 10^{-5}$ cm^{-3}
10^{-2} (30 Mpc)	0.50	0.29	0.17	
10^{-1}	0.76	0.56	0.39	$N_e < 10^{-5}$ cm^{-3}

a) $s = $ (correlation length of antimatter region) $\times H/c$ with $H = 100$ km sec^{-1} Mpc^{-1}, the Hubble constant.

We have estimated upper limits on the amount of antimatter in the space from $z = 0$ to $z = 2$ and concluded that the intergalactic space up to $z = 2$ is not symmetric with respect to matter and antimatter. Particularly if the correlation length of the antimatter region, s, is equal to or larger than the diameter of the supercluster of galaxies, the ratio η amounts to 0.4 or more; the space up to $z = 2$ must be filled dominantly with matter or antimatter alone.

On the other hand, if the universe is symmetric with respect to matter and antimatter, and if the linear relation between R.M. and $z \cdot \cos\theta$ is accidental according to slight deviation from the symmetry in the space up to $z=2$ ($0.5 > \bar{a} > 0.49$, or $0.0 < \eta < 0.02$, say), the relation $N_e B = \eta^{-1} \times 2 \times 10^{-14}$ and and $B < 2 \times 10^{-8}$ gauss lead us to the closed universe with $N_{|e|} > 5 \times 10^{-5}$ cm^{-3} or $\rho > 8 \times 10^{-29}$ gr cm^{-3}.

We can neither reject nor support the presence of antimatter. However, the method developed so far seems very promising for determining upper limits on the amount of antimatter when more observational materials are accumulated in future on the Faraday rotations of extragalactic radio sources, background non-thermal radio emissions and diffuse X-rays.

We stop here our discussions on magnetic fields at the level of the universe. The follwoing three sections will be devoted to problems of magnetic fields in the Galaxy and galaxies.

§4. Helical magnetic fields in the spiral arm

4-1 *Equations of motion of magnetized interstellar gas in a model spiral arm*

As introduced in §1, the helical model is a most plausible description of interstellar magnetic field in the Galaxy, interpreting satisfactorily distributions of polarization planes of starlight and of rotation measures of polarized extragalactic radio sources (Behr 1959; Hoyle and Ireland 1961; Ireland 1961; Stępién 1964; Hornby 1966; Bingham and Shakeshaft 1967; and Mathewson 1968). In the present section we investigate magneto-hydrodynamical behavior of interstellar gas in a model arm and attempt to find a condition that a helical magnetic field can be in a stationary state without being sheared to lose its identity by galactic differential rotation (Fujimoto and Miyamoto 1969, 1970).

A circular arm with elliptical cross-section is used as a model of the spiral arm[*] (Fig. 10). A rotating cylindrical system of coordinates (r, φ, z) with the origin at the galactic center is chosen in which the longitude φ increases in the direction of galactic rotation. The z-axis coincides with the symmetry axis of the Galaxy, and galactic plane is defined by $z=0$. The time-independent equations of motion of gaswith ʰinfinite conductivity are given by

---

[*] The spiral arm is widely accepted as due to density wave of galactic disk (see I.A.U. Symposium No. 38 edited by Becker and Contopoulos, 1970). The present model is taken so as to show that a rolling (screw) motion of gas around the arm axis is dynamically permissible.

$$(\boldsymbol{U} \cdot \boldsymbol{V}) \boldsymbol{U} = 2\boldsymbol{U} \times \boldsymbol{\Omega} - \frac{1}{\rho_s} \boldsymbol{V} P - \boldsymbol{V} \left(\boldsymbol{\Phi}_G + \boldsymbol{\Phi}_s - \frac{r^2}{2} \boldsymbol{\Omega}^2 \right) + \frac{\mathrm{rot}\, \boldsymbol{B} \times \boldsymbol{B}}{4\pi\rho_s} , \qquad (4 \cdot 1)$$

$$\boldsymbol{V}^2 (\boldsymbol{\Phi}_G + \boldsymbol{\Phi}_s) = 4\pi G (\rho_s + \rho_G), \qquad (4 \cdot 2)$$

$$\mathrm{div}\, \boldsymbol{B} = 0, \qquad (4 \cdot 3)$$

$$\mathrm{div}\, (\rho_s \boldsymbol{U}) = 0, \qquad (4 \cdot 4)$$

$$\mathrm{rot}\, (\boldsymbol{U} \times \boldsymbol{B}) = 0, \qquad (4 \cdot 5)$$

with

$$\boldsymbol{\Omega} = \Omega \boldsymbol{e}_z .$$

Here $\boldsymbol{\Omega}$ is the angular velocity of the rotating coordinates system, ρ_G the density of overall axisymmetric mass distribution in the smoothed Galaxy, ρ_s the gaseous density of the spiral arm, $\boldsymbol{\Phi}_G$ and $\boldsymbol{\Phi}_s$ the corresponding gravitational potentials. The unit vector $\boldsymbol{e}_z$ points the direction of the z-axis. Other symbols have their usual meanings.

We take a circular arm whose characteristic scale of

Fig. 10. A local Cartesian coordinates system (x, y, z), stream lines and magnetic lines of force around the arm axis.

the cross-section is much smaller than that of the Galaxy, and consider a case that the motion of gas in the arm is axisymmetric about the z-axis, i.e., that every quantity is independent of φ. It will prove convenient to introduce a local Cartesian coordinates system (x, y, z) with the origin at $(r_0, \varphi_0, 0)$; $z = z$, the x-axis is directed towards the galactic anticenter, and the y-axis is parallel to the arm (see Fig. 10). This Cartesian coordinates system rotates with a local angular velocity of galactic rotation at $r = r_0$,

$$\Omega^2 = \left(\frac{1}{r} \frac{\partial \boldsymbol{\Phi}_G}{\partial r} \right)_{\substack{r=r_0 \\ z=0}}. \qquad (4 \cdot 6)$$

Since the characteristic scale of the arm's cross-section is much smaller than that of the Galaxy, we can expand the gravitational force in a Taylor series around the arm axis. It is sufficient to take the following terms,

$$\boldsymbol{V} \boldsymbol{\Phi}_G = \left(\frac{\partial \boldsymbol{\Phi}_G}{\partial r} , \frac{\partial \boldsymbol{\Phi}_G}{r \partial \varphi} , \frac{\partial \boldsymbol{\Phi}_G}{\partial z} \right)$$

$$= \left(\left(\frac{\partial \boldsymbol{\Phi}_G}{\partial x} \right)_0 + x \left(\frac{\partial^2 \boldsymbol{\Phi}_G}{\partial x^2} \right)_0 , 0 , z \left(\frac{\partial^2 \boldsymbol{\Phi}_G}{\partial z^2} \right)_0 \right), \qquad (4 \cdot 7)$$

where a subscript 0 is attached to quantities evaluated at $(r_0, \varphi_0, 0)$, and we have made a reasonable assumption that Φ_G is separable in x and z near the galactic plane. The similar series expansion is applicable to Φ_s. If we assume a circular arm whose density ρ_s is uniform and whose cross-section is elliptical with semi-major axis, a, parallel to the galactic plane and semi-minor axis, b, perpendicular to it, we have the following asymptotic expression for Φ_s (Lamb 1945)

$$\Phi_s = \text{const} + 2\pi G \rho_s \left(\frac{bx^2 + az^2}{a+b} \right) \quad \text{for} \quad S \geq 0, \tag{4·8}$$

with

$$S = 1 - (x^2/a^2) - (z^2/b^2). \tag{4·9}$$

When $B = 0$, the gaseous pressure in the arm may be represented by

$$P = P_c S, \tag{4·10}$$

where P_c is the pressure at the arm axis.

(a)   Hydrodynamical motion of gas in the arm $(B=0)$

    When a and $b \ll r_0$, we have $|\text{grad}| \gg 1/r$ and $|U| \ll \Omega r$ for the gas of $S \geq 0$. Hence, the time- and φ (or y)-independent equation of motion of non-magnetized gas can be written in terms of the local Cartesian coordinates. Substitutions of Eqs. (4·2) and (4·6) ~ (4·10) in Eqs. (4·1) and (4·4) yield

$$U_x \frac{\partial U_x}{\partial x} + U_z \frac{\partial U_x}{\partial z} = 2\Omega U_y - Lx, \tag{4·11}$$

$$U_x \frac{\partial U_y}{\partial x} + U_z \frac{\partial U_y}{\partial z} = -2\Omega U_x, \tag{4·12}$$

$$U_x \frac{\partial U_z}{\partial x} + U_z \frac{\partial U_z}{\partial z} = -Mz \tag{4·13}$$

and

$$\frac{\partial U_x}{\partial x} + \frac{\partial U_z}{\partial z} = 0, \tag{4·14}$$

where L and M are constants which include various parameters in Eqs. (4·7), (4·8) and (4·10)

$$-Lx \equiv -\frac{1}{\rho_s} \frac{\partial P}{\partial x} - \frac{\partial}{\partial x} \left(\Phi_G + \Phi_s - \frac{r^2}{2} \Omega^2 \right)$$

$$= -\left(r_0 \frac{\partial}{\partial r} \left(\frac{1}{r} \frac{\partial \Phi_G}{\partial r} \right)_0 - \frac{2P_c}{\rho_s a^2} + \frac{4\pi G \rho_s b}{a+b} \right) x \tag{4·15}$$

and

$$-Mz \equiv -\frac{1}{\rho_s}\frac{\partial P}{\partial z} - \frac{\partial}{\partial z}(\Phi_G + \Phi_R)$$

$$= -\left(\left(\frac{\partial^2 \Phi_G}{\partial z^2}\right)_0 - \frac{2P_c}{\rho_R b^2} + \frac{4\pi G \rho_R a}{a+b}\right)z. \qquad (4\cdot16)$$

We look for a velocity field in the following form with still unspecified numbers A_{ij},

$$\begin{pmatrix} U_x \\ U_y \\ U_z \end{pmatrix} = \begin{pmatrix} A_{11} & 0 & A_{13} \\ A_{21} & 0 & A_{23} \\ A_{31} & 0 & A_{33} \end{pmatrix}\begin{pmatrix} x \\ y \\ z \end{pmatrix}, \qquad (4\cdot17)$$

where $A_{12}=A_{22}=A_{32}=0$ are due to the assumption of axisymmetric motion of gas about the axis of the Galaxy. Since the streamlines of the arm gas never cross over the arm surface, $(U\cdot\mathrm{grad})S=0$, we have

$$\frac{U_z}{U_x} = -\frac{b^2 x}{a^2 z},$$

or from Eq. (4·17),

$$\frac{A_{31}}{A_{13}} = -\frac{b^2}{a^2} \qquad (4\cdot18)$$

and

$$A_{11} = A_{33} = 0. \qquad (4\cdot19)$$

Hence Eq. (4·14) is automatically satisfied. Substitutions of Eqs. (4·17), (4·18) and (4·19) in (4·11)~(4·13) yield

$$A_{13}A_{31} = 2\Omega A_{21} - L, \qquad (4\cdot20)$$

$$A_{13}A_{21} = -2\Omega A_{13}, \qquad (4\cdot21)$$

$$A_{13}A_{31} = -M \qquad (4\cdot22)$$

and

$$A_{23} = 0. \qquad (4\cdot23)$$

Equations (4·18), (4·21) and (4·22) give nonzero elements immediately,

$$A_{13} = \pm (a/b)M^{1/2}, \qquad (4\cdot24)$$

$$A_{21} = -2\Omega \qquad (4\cdot25)$$

and

$$A_{31} = \mp (b/a)M^{1/2}. \qquad (4\cdot26)$$

Equations (4·20), (4·22) and (4·25) impose a constraint on L and M,

$$L - M = -4\Omega^2. \qquad (4\cdot27)$$

Equations (4·20) and (4·21) represent a motion of a gaseous element projected onto the galactic plane, which is, when $P_c = \rho_8 = 0$, identical with an epicyclic motion of a star with small amplitude. Equation (4·22) represents a periodic motion perpendicular to the galactic plane. The constraint (4·27) implies that the frequencies of these periodic motions must be the same for a steady flow of gas in the arm; the streamlines are closed, seen in the rotating frame.

The motion of the gas, $U_x = A_{13} z$, $U_y = A_{21} x$ and $U_z = A_{31} x$, represents a screw (or rolling) motion along the arm when observed from an inertial frame. As shown in Eqs. (4·24) and (4·26), A_{13} and A_{31} can be both positive and negative. The rolling motion of $A_{13} = (a/b) M^{1/2}$ and $A_{31} = -(b/a) M^{1/2}$ is in a counterclockwise sense and that of $A_{13} = -(a/b) M^{1/2}$ and $A_{31} = (b/a) M^{1/2}$ is in a clockwise sense viewed along the y-axis (Fig. 10). It is to be noted that the rolling motion is not always associated with helical magnetic fields. If the following characteristics are taken as a model spiral arm,

$$
\left.
\begin{array}{l}
r_0 = 10 \text{ kpc}, \quad \Omega = 8.1 \times 10^{-16}/\text{sec} \, (\, T = 2\pi/\Omega = 2.4 \times 10^8 \text{ yrs}), \\[2mm]
\left(\dfrac{\partial^2 \Phi_G}{\partial z^2} \right)_0 = 8.2 \times 10^{-30}/\text{sec}^2 \text{ (Oort 1965)}, \quad \rho_8 = 3.4 \times 10^{-24} \text{ gr/cm}^3, \\[2mm]
a = 250 \text{ pc} \quad \text{and} \quad b = \tfrac{1}{3} a,
\end{array}
\right\} \quad (4\cdot28)
$$

and if we follow the galactic rotation law derived from the λ 21-cm line survey (Schmidt 1965), we have numerical solutions in the second column of Table IV. If the pressure is due to random motion of gas clouds, the root-mean square velocity at the arm axis is of the order of

$$
\sqrt{\langle V_t^2 \rangle} \sim \sqrt{P_c/\rho_8} = 9.5 \text{ km/sec}.
$$

(b) Magneto-hydrodynamical motion of gas in the arm, $\boldsymbol{B} \neq 0$

We have found a screw motion of gas along the arm with no magnetic field. It is obvious that if magnetic lines of force run parallel to the local streamlines of the screw motion $(A_{13} z, \; A_{21} x + r_0 \Omega, \; A_{31} x)$, they are in a stationary state, because Eqs. (4·3) and (4·5) are automatically satisfied. However such field lines are not so tightly wound as concluded from the helical model discussed in §1. The present subsection is devoted to constructing time-independent magneto-hydrodynamical models of the following tightly wound helical field,

$$
\boldsymbol{B} = (B_* A_{13} z, \; B_0 + B_* A_{21} x, \; B_* A_{31} x) \qquad \text{for} \quad S > 0 \qquad (4\cdot29)
$$

and

$$
= 0 \qquad\qquad\qquad\qquad\qquad\qquad \text{for} \quad S < 0, \qquad (4\cdot30)
$$

together with

$$U = (A_{13}z, \ A_{21}x, \ A_{31}x), \tag{4·31}$$

where A_{13}, A_{21}, A_{31} and B_* are to be determined by the equation of motion and B_0 means a uniform longitudinal field along the arm. The helical field (4·29) and the rolling motion (4·31) obviously satisfy Eqs. (4·3) and (4·5) in the local coordinates system where $1/r \ll |\mathrm{grad}|$ and $|U| \ll \Omega r$ hold as before. One finds immediately that the helical field (4·29) is not parallel to the streamline of the screw motion seen from the inertial frame.

The acceleration due to the Lorentz force is written by using Eq. (4·29),

$$\frac{1}{4\pi\rho_\mathrm{s}} \mathrm{rot}\, \boldsymbol{B} \times \boldsymbol{B}$$

$$= \left[\frac{B_*^2 \{A_{31}(A_{13} - A_{31}) - A_{21}^2\}}{4\pi\rho_\mathrm{s}} x - \frac{B_0 B_* A_{21}}{4\pi\rho_\mathrm{s}}, \right.$$

$$\left. \frac{B_*^2 A_{13} A_{21} z}{4\pi\rho_\mathrm{s}}, \ \frac{B_*^2 A_{13}(A_{31} - A_{13})z}{4\pi\rho_\mathrm{s}} \right]. \tag{4·32}$$

A constant acceleration, $B_0 B_* A_{21}/4\pi\rho_\mathrm{s}$, in Eq. (4·32) can be eliminated by choosing the angular velocity of the local coordinates system such that

$$r_0 \Omega^2 = \left(\frac{\partial \Phi_\mathrm{G}}{\partial r} \right)_0 + \frac{B_0 B_* A_{21}}{4\pi\rho_\mathrm{s}}. \tag{4·33}$$

Even if we take $B_* A_{21} \sim 10^{-5}$ gauss/250 pc which is currently regarded as an upper limit, $B_0 \sim 5 \times 10^{-7}$ gauss which is evaluated for the tightly wound helical field, and $\rho_\mathrm{s} = 2$ hydrogen atoms/cm³, the second term on the right-hand side of Eq. (4·33) amounts to only one percent of the first term. In what follows, therefore, we neglect this term and adopt the same angular velocity as in the preceding hydrodynamical treatment.

The helical magnetic field (4·29) and (4·30) generate the surface current $\boldsymbol{J}_s$ at $S=0$, which exerts a force, coupled with $\boldsymbol{B}$, normal to the arm surface. That is

$$\frac{1}{2} \boldsymbol{J}_s \times \boldsymbol{B} = \frac{1}{8\pi} \{(B_0 + B_* A_{21}x)^2 + B_*^2 (A_{31}x^2 + A_{13}^2 z^2)\} \boldsymbol{n}, \tag{4·34}$$

where $\boldsymbol{n}$ is a unit vector normal to the arm surface and points outwards. The terms associated with B_0 are very small compared with other terms when the helical field is much wound. We neglect these terms and write the pressure as

$$P = P_c \left(1 - \frac{x^2}{a^2} - \frac{z^2}{b^2} \right) - \frac{1}{2} |\boldsymbol{J}_s \times \boldsymbol{B}|$$

$$= P_c \left(1 - \frac{x^2}{a^2} - \frac{z^2}{b^2} \right) - \frac{B_*^2}{8\pi} (A_{21}^2 x^2 + A_{31}^2 x^2 + A_{13}^2 z^2), \tag{4·35}$$

where we have assumed an incompressible gas.

Adding Eq. (4·32) to the right-hand sides of Eqs. (4·11)∼(4·13), re-writing the pressure in Eqs. (4·15) and (4·16) by using Eq. (4·35), and finally putting Eq. (4·31) into the left-hand sides of Eqs. (4·11)∼(4·13), we have three equations corresponding to Eqs. (4·20)∼(4·22)

$$A_{13}A_{31} = 2\Omega A_{21} - L + \frac{B_*^2}{4\pi\rho_s} A_{13}A_{31} , \tag{4·36}$$

$$A_{13}A_{21} = -2\Omega A_{13} + \frac{B_*^2}{4\pi\rho_s} A_{21}A_{13} \tag{4·37}$$

and

$$A_{13}A_{31} = -M + \frac{B_*^2}{4\pi\rho_s} A_{13}A_{31} , \tag{4·38}$$

where L and M are identical with those in Eqs. (4·15) and (4·16). When $A_{13} \neq 0$ and $B_*/4\pi\rho_s \neq 1$, Eqs. (4·37) and (4·38) give nonzero elements,

$$A_{13} = \pm (a/b)M^{-1/2}\left(1 - \frac{B_*^2}{4\pi\rho_s}\right)^{-1/2} , \tag{4·39}$$

$$A_{21} = -2\Omega\left(1 - \frac{B_*^2}{4\pi\rho_s}\right)^{-1} \tag{4·40}$$

and

$$A_{31} = \mp (b/a)M^{-1/2}\left(1 - \frac{B_*^2}{4\pi\rho}\right)^{-1/2} , \tag{4·41}$$

with a constraint for the model arm corresponding to Eq. (4·27),

$$L - M = -4\Omega^2\left(1 - \frac{B_*^2}{4\pi\rho}\right)^{-1} . \tag{4·42}$$

It is clear that when $B_* = 0$ all these solutions are reduced to the ones obtained in the hydrodynamical treatment.

We have the following relation

$$B_*^2/4\pi\rho_s \equiv \frac{1}{8\pi}\{(B_*A_{31}x)^2 + (B_*A_{13}z)^2\} \Big/ \frac{\rho_s}{2}\{(A_{31}x)^2 + (A_{13}z)^2\}$$

$$= \frac{\textit{Energy density of the magnetic field projected onto a plane perpendicular to the arm axis}}{\textit{Energy density of the rolling motion projected onto a plane perpendicular to the arm axis}} .$$

Table IV lists numerical solutions for the characteristics of the model arm (4·28) and various values of $B_*^2/4\pi\rho_s$.

Table IV. Velocities of rolling motions of gas and helical magnetic fields for various values of $B_*^2/4\pi\rho_s$.

	$B_*^2/4\pi\rho_s$				
	0.0	0.1	0.3	0.5	0.7
U_x	$\pm 8.0z$ km s^{-1}	$\pm 10.0z$	$\pm 15.5z$	$\pm 25.1z$	$\pm 46.6z$
U_y	$-5.0z$	$-5.5x$	$-7.1x$	$-10.0x$	$-16.7x$
U_z	$\mp 0.9x$	$\mp 1.1x$	$\mp 1.7x$	$\mp 2.8x$	$\mp 5.2x$
B_x	0	$\pm 2.1\times 10^{-6} zG$	$\pm 5.6\times 10^{-6} z$	$\pm 1.2\times 10^{-5} z$	$\pm 2.6\times 10^{-5} z$
B_y	0	$-1.1\times 10^{-6} x$	$-2.6\times 10^{-6} x$	$-4.6\times 10^{-6} x$	$-9.1\times 10^{-6} x$
B_z	0	$\mp 2.3\times 10^{-7} x$	$\mp 6.2\times 10^{-7} x$	$\mp 1.3\times 10^{-6} x$	$\mp 2.8\times 10^{-6} x$
$\sqrt{\langle V_t^2\rangle}$	9.5 km s^{-1}	9.5	9.1	8.1	5.2

(1) x and z are measured in 100 pc; (2) $\sqrt{\langle V_t^2\rangle}$ is the root-mean square molecular (or random) velocity of the gas at the arm axis; (3) the constant B_* is taken as positive. When it is negative, the signs in B_x, B_y and B_z are to be reversed.

4-2 Comparisons with observations

The helical magnetic field in the spiral arm has been discussed to be a dynamically permissible configuration, if a rolling motion of gas is superimposed on galactic rotation. If we are at an inner side of our model spiral arm and observe from within the linearly polarized radio emission of extragalactic radio sources near galactic plane, we can expect a large amount of Faraday rotation due to a stratified magnetized plasma in the Galaxy and sign reversals of the rotation measures above and below the galactic plane at particular galactic longitudes, $l\approx 0°$ and $l\approx 180°$. On the other hand, when we measure optical polarization of stars in the present model spiral arm, an electric vector (therefore, a magnetic line of force projected onto the sky, if we follow Davis and Greenstein (1951)) are nearly parallel to the galactic plane, and perpendicular to it at $l\approx 90°$ and $l\approx 270°$.

These results may be regarded as qualitatively compatible with the observed distributions of the rotation measures of polarized extragalactic radio sources (Morris and Berge 1964; Gardner and Davies 1966; Berge and Seielstad 1967; and Gardner, Whiteoak and Morris 1967), and of starlight polarization planes, but they cannot explain the field structure pointed out by Hornby (1966) and Mathewson (1968) that the helical field is sheared through an angle of 40° in the galactic plane.

Lindblad (1967) and Velden (1970) have observed the λ 21-cm line emission of neutral hydrogen gas around the galactic anticenter, where non-circular motion of gas has been observed explicitly. They have found that the gas at $b>0$ is approaching us, while the one at $b<0$ is receding from us with a speed of several km/sec, respectively. If we look this motion in an inertial frame, it is nothing but a screw motion schematically shown in Fig. 10. These

two observations support our conclusion on the rolling motion of gas, at least, for the gas at $l \approx 180°$ and $-4° > b > -16°$ (Lindblad 1967) or for the one at $l \approx 180°$ and $10° < |b| < 30°$ (Velden 1970).

In the next section, we discuss more extensively the rolling motion in other galactic longitude ranges on the basis of the λ 21-cm line survey of galactic plane by Westerhout (1966, 1969).

§5. Rolling motions and eddy structures of neutral hydrogen gas in the spiral arm

5-1   *Observations of rolling motions*

It has been clarified both theoretically and observationally that the helical magnetic field is deeply associated with rolling motions of gas in the spiral arm. A rolling motion of interstellar neutral hydrogen gas was first observed by Rougoor (1964), although no dynamical discussions have been made about it. Kerr (1969) and Burton (1970) have confirmed the rolling motion of neutral hydrogen gas in other galactic longitude ranges. Kerr (1970) has also suggested that these effects may be related to helical magnetic field patterns in spiral arms.

In the present section we investigate in more details how the rolling motion is distributed in the Galaxy (Fujimoto and Tanahashi 1971). The observational data are due to the λ 21-cm line survey of galactic plane by Westerhout (1966, 1969), which cover $l = 11° \sim 235°$ and are arranged in the form of iso-brightness contours as a function of radial velocity and galactic latitude, or in the (V_r, b)-plane. Figure 11 is a typical example of the iso-brightness contour map at $l = 143°20'$, in which one finds three arms at V_r $= -16$, -42 and -70 km/sec. The inclinations of the shaded parts indicate the presence of rolling motions around the arm axes. We define the magni-
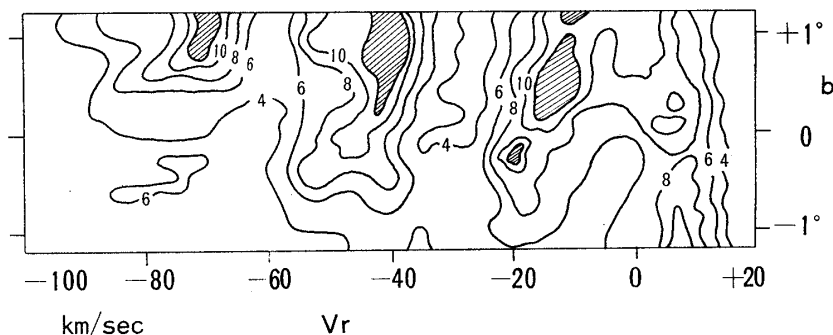

Fig. 11. Iso-brightness contour map of neutral hydrogen gas in the (V_r, b)-plane at $l = 143°20'$ (Westerhout 1966, 1969). The shaded regions indicate the maximum brightness in the spiral arms at $V_r = -16$, -42 and -70 km/sec, where V_r denotes the radial velocity of the hydrogen gas. The bright region at $V_r = -42$ km/sec is the Perseus arm whose rolling motion at $l = 30°$ to $90°$ is given in Fig. 12.
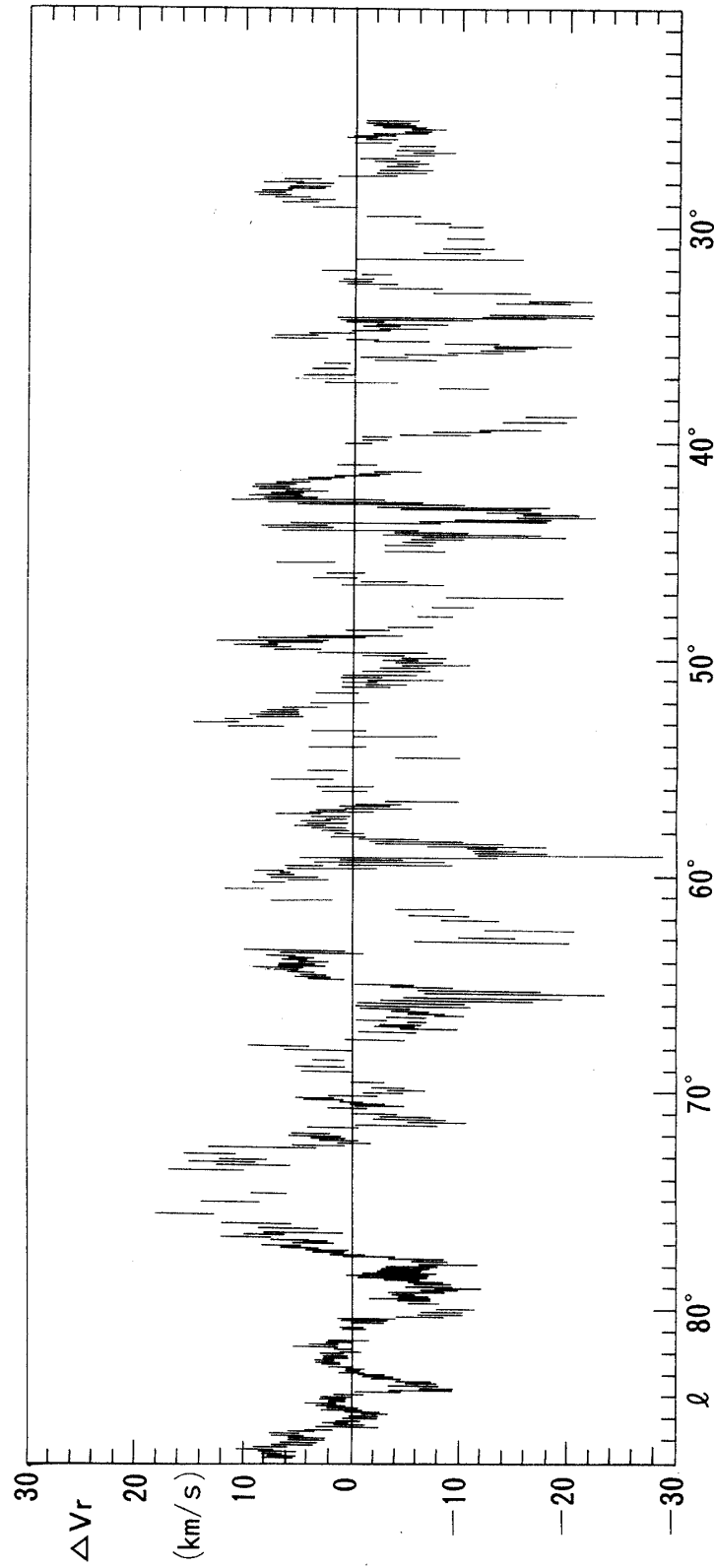
Fig. 12. Rolling motions of neutral hydrogen gas along the Perseus arm (I). Vertical bars indicate maximum errors possible in eye-estimates of the data.

tude of the rolling motion by

$$\Delta V_r = V_r^{(+)} - V_r^{(-)}$$

$$(= 2dV_r/db),$$

(5·1)

where $V_r^{(+)}$ and $V_r^{(-)}$ designate the line-of-sight components of the motion of neutral hydrogen gas at $b=1°$ and $-1°$ in the spiral arm, respectively. We plot ΔV_r along the Perseus and distant arms (Figs. 12 and 13) which show the presence of the rolling motion in every spiral arm. Although the λ 21-cm line survey by Westerhout (1966, 1967) does not cover all galactic longitudes, we can regard the rolling motion as a general dynamical phenomenon in the gaseous arm of the Galaxy.

The distribution diagrams of ΔV_r give us many characteristics of the rolling motion. (i) The sense of the rolling motion changes from place to place along the arm (Kerr 1970). Indeed we have $\Delta V_r > 0$ at $l = 72° - 77°$,
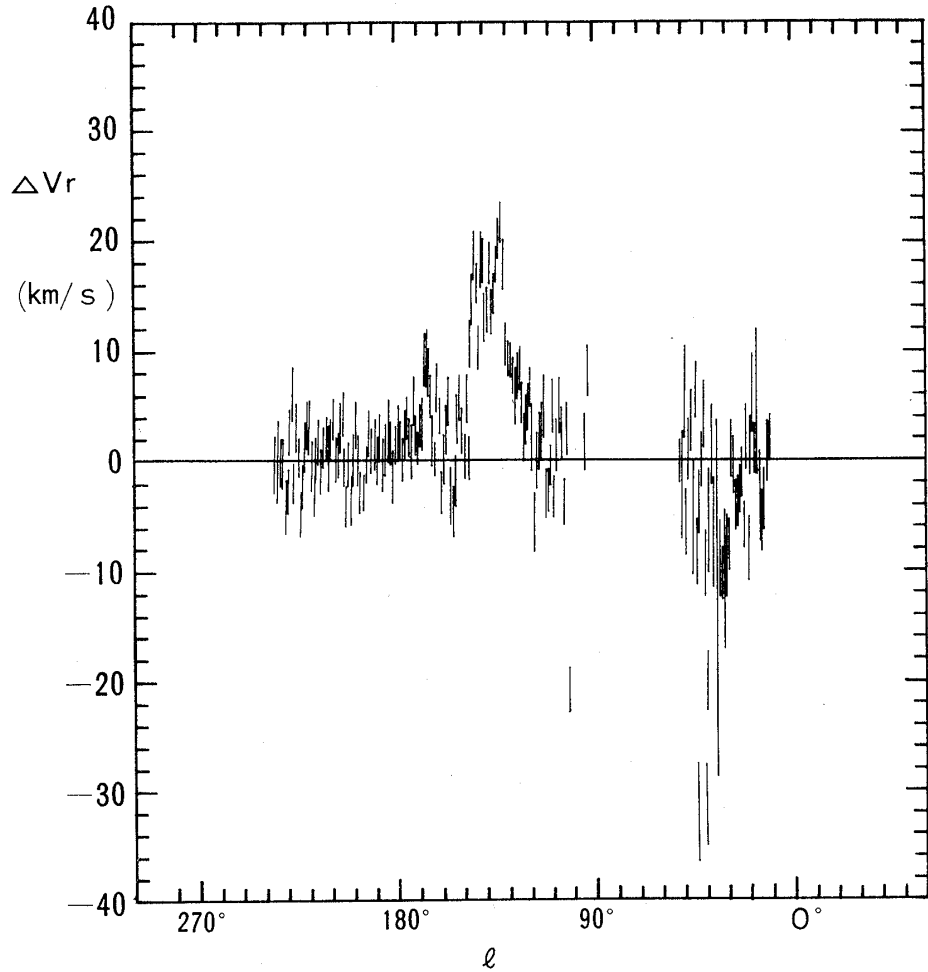

Fig. 13. Same as Fig. 12, but along the distant arm (II) which is situated next to the Perseus arm. Note that the unit of the horizontal axis is ten times the one in Fig. 12.

$\Delta V_r < 0$ at $l = 78° - 81°$ and $\Delta V_r > 0$ at $l = 81° - 83°$ etc. in the Perseus arm (I). A typical correlation length of ΔV_r is about 300 pc along the arm. (ii) Some isolated distributions of ΔV_r are found at $l = 45°$ and at $l = 103°$ in the distant arm (II). These facts lead us to conclude that the rolling motion is essentially inhomogeneous. (iii) Some large rolling motions have been found locally along the arms. (iv) The observed inclinations of the iso-brightness contours dV_r/db is nearly constant for $|b| < 1°$ (see Fig. 11), indicating that the velocity of the rolling motion increases in a linear fashion away from the arm axis.

5-2 *Nonuniform rolling motions of interstellar gas and possible formation of helical magnetic fields*

In our dynamical treatment of the rolling motion of gas in the model arm, we have shown that all gaseous elements perform an epicyclic motion parallel to galactic plane and a periodic motion perpendicular to it, with the same period (see Eqs. (4·27) and (4·42)). As discussed in 4-1, the rolling motions, $\Delta V_r > 0$ and $\Delta V_r < 0$, are dynamically permissible in the model arm.

The distribution of ΔV_r has been found to be nonuniform and to change rapidly along the arm. This tendency is contrary to the model in §4 where we have taken that every dynamical quantity remains unchanged along the same arm.

Now these facts conclude that the rolling motion is intrinsically non-uniform and our theoretical result in §4 holds only in local small regions along the arm. If this idea is accepted, a still open problem on a formation of the helical field can be resolved naturally. Because the presence of longitudinal component of magnetic field is observationally certain, the nonuniform rolling motion must generate poloidal component where $|d\Delta V_r/dl|$ is large, and form helical field patterns eventually. According to the density wave theory of the spiral arm (Lin and Shu (1964) and see IAU Symp. No. 38 edited by Becker and Contopoulos 1970), the disk gas in galactic rotation catches up to the spiral pattern, being compressed and staying there for $10^{7 \sim 8}$ years (near the sun), and then leave it. A simple calculation shows that a typical value of $|d\Delta V_r/dl|$ observed in Figs. 12 and 13 is sufficiently large to generate the helical field with a pitch angle of $1° \sim 10°$ in this time interval. This pitch angle is comparable to the one determined by Hornby (1966) and Mathewson (1968).

Indeed, inhomogeneous rolling motions in the solar neighborhood are seen in Fig. 2 in a paper by Velden (1970) and also in Fig. 4 by Fujimoto and Tanahashi (1971). Velden has observed radial velocities of neutral hydrogen at intermediate latitudes $b = 10° \sim 30°$ and $b = -10° \sim -30°$ along galactic longitude $l = 120°$ to $240°$, where one finds $\Delta'V_r = V_r(b = 10° \sim 30°) - V_r(b = -10° \sim -30°)$ is negative and finite at $l = 160° \sim 210°$. It is to be noted that $|\Delta'V_r|$ attains its maximum value 9 km/sec at $l = 180° \sim 190°$ and tends

to zero rapidly at $l=160°$ and $l=210°$. These facts clearly show the presence of inhomogeneous rolling motions in the solar neighborhood.

In view of the distribution diagrams of ΔV_r and of this formation mechanism of helical magnetic field, we feel that the distribution of ΔV_r has an aspect of magneto-hydrodynamical turbulence with a typical wave length of 300 pc, and that local helical pattern is an ordinary configuration prevailing over the entire Galaxy.

From their investigations of distribution of rotation measures for polarized extragalactic radio sources, Mathewson and Nicholls (1968) has suggested that the helical magnetic field may be a local phenomenon in the solar neighborhood with a scale of 500 pc. Dispersions of the arrival time and rotation measures of polarized pulsar signals are statistically analyzed by Jokippii and Lerche (1969), concluding that the interstellar electron and magnetic field are in a random distribution with a correlation length of about 200 pc. On the other hand, Parker (1969) worked out theoretically the field amplification in the turbulent magnetized interstellar gas and concluded that the characteristic sky distribution of rotation measures of polarized extragalactic radio sources can be explained by the random walk of turbulent eddies with typical diameters of 400 pc. It is interesting to note that these wave lengths, 200 pc of Jokippii and Lerche, 500 pc of Mathewson and Nicholls and 400 pc of Parker are of the same magnitude as the correlation length of 300 pc observed in the distribution of ΔV_r, and that they much exceed the diameter of interstellar gas cloud of about 10 pc.

In the next subsection, these larger eddies found in the distribution diagrams of ΔV_r will be confirmed as real structures in the Galaxy.

5-3   Eddy structures and spin motions of interstellar hydrogen gas

The eddy wave length (in degree) of ΔV_r along the arm can be obtained after finding the position (in l) at which ΔV_r changes appreciably. The eddies thus estimated are indicated by the dashed lines along the Sagittarius arm (Fig. 14).

The line-of-sight velocity of hydrogen gas, V_r, at the axis of the Sagittarius arm is given in Fig. 14 as a function of l. Wavy structures δV_r are found superimposed on the smoothed curve $(\overline{V}_r)$ of V_r. Comparing the eddies in ΔV_r and in δV_r, we find strikingly good coincidences between them; the fluctuations δV_r always take place where ΔV_r changes rapidly.[*] Cases of no coincidence are exceptional. As defined in Eq. (5·1), the rolling motion ΔV_r is the difference between the line-of-sight components of motion of gas at $b=1°$ and $b=-1°$ at a particular galactic longitude considered, representing the rotation of gas around the arm axes, whereas δV_r implies deviations from circular motion of gas in the galactic plane.

---

[*] Fujimoto and Tanahashi have made this analysis. We thank Mr. Tanahashi for permitting us to use the results before publication.

Because ΔV_r and δV_r are dynamically independent of each other, the good coincidence between the eddies of δV_r and ΔV_r represents a real existence of larger gaseous eddies whose typical diameters are hundreds pc.

The overall smoothed curve $\overline{V}_r$ of radial velocity usually leads to a galactic rotation law. Let us look the eddies in the upper diagram of Fig. 14, then we find that dV_r/dl evaluated in each eddy does not coincide with $d\overline{V}_r/dl$ at the corresponding position; $dV_r/dl > d\overline{V}_r/dl$ in E_1, $dV_r/dl < d\overline{V}_r/dl$ in E_2 and $dV_r/dl > d\overline{V}_r/dl$ in E_3, for example. These differences between $d\overline{V}_r/dl$ and dV_r/dl indicate the presence of an intrinsic rotation of the eddy, superposed on local galactic rotation. Now, combining the rolling motion ΔV_r (the lower diagram of Fig. 14) and the intrinsic rotation of the eddy, $(dV_r/dl - d\overline{V}_r/dl)$, we can conclude that the eddy of diameter of hundreds
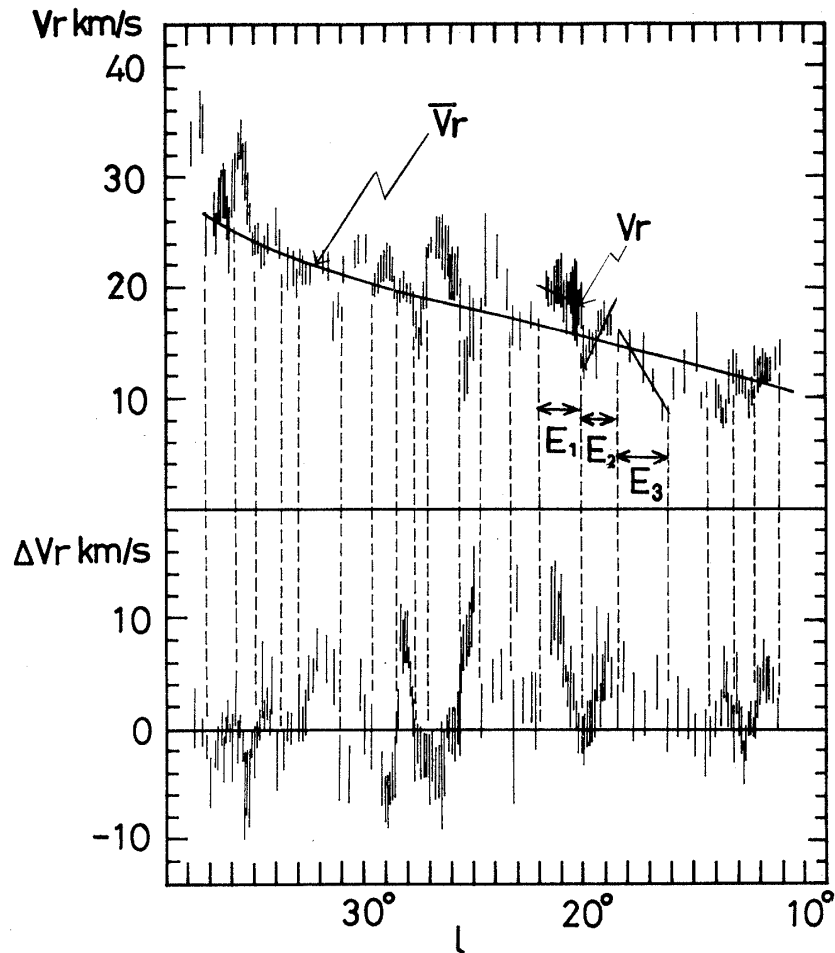

Fig. 14. Fine structures in distribution diagrams of the radial velocity of gas at the axis of the Sagittarius arm and of the rolling motion ΔV_r in the same arm. Good coincidences are found between the fluctuations in V_r and those in ΔV_r. Note that dV_r/dl evaluated in each eddy is observed to be different from $d\overline{V}_r/dl$ evaluated at the corresponding longitude, where $\overline{V}_r$ is an overall smoothed curve of V_r which usually leads to a galactic rotation law.

pc performs an intrinsic spin motion whose vector is distributed in a random fashion in its magnitude and direction.

At the end of this section, we conclude the following description of interstellar gas and magnetic field in the Galaxy. The spiral arm is lined successively with large gaseous clouds with a typical diameter of 300 pc, and each cloud is spinning with a period of 5×10^7 years superimposed on galactic rotation. The vector of the spin is distributed in a random fashion in its magnitude and direction. Since the magnetic line of force is frozen in interstellar gas, the field line must be distorted helically between the spinning eddies where $|d\Delta V_r/dl|$ is large. In view of the nonuniform distribution of ΔV_r along the arm, helical patterns must be a common feature in magnetic fields in the Galaxy (see schematic structures of a representative magnetic line of force in Fig. 15). The magneto-hydrodynamical treatment in §4 may not hold for the actual problem in its present form (compare Figs. 10 and 15), but it has served to develope the discussions in §5, and if we apply it to local motions of gas, we can understand dynamical meanings of the rolling motions of $\Delta V_r > 0$ and $\Delta V_r < 0$.
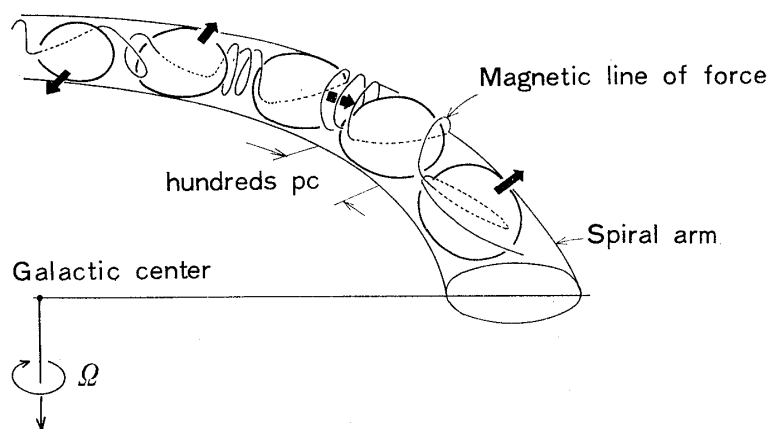

Fig. 15. A model of spinning gaseous clouds in a spiral arm. Vectors of the spin (dark arrow) are distributed at random in magnitude and direction. A representative magnetic line of force is distorted between the spinning clouds.

§6. Magneto-hydrodynamical studies of magnetic fields in the barred galaxy

6-1 *Equations of motion of magnetized gas in a model barred galaxy*

Visvanathan (1968), Mathewson and Ford (1970), and Schmidt (1970) have measured optical polarization planes of stars and emission regions in the Large and Small Magellanic Clouds and in the space enveloping these two nebulae. If we follow Davis and Greenstein (1951), the topology of magnetic lines of force can be obtained. The present section is devoted to dynamical studies of magnetic fields in the Magellanic-type barred galaxy, referring to

Mathewson and Ford's observations of starlight polarizations in the bar of the LMC. We take the following basic assumptions. (1) The barred galaxy can be described by Freeman's ellipsoidal stellar system (1966) of uniform density rotating end over end. (2) Magnetized interstellar gas is embedded in Freeman's model, and the gravitational force is due to the mass of member stars, or the gravitational force due to the gas is negligibly small. (3) Magnetic fields and internal motions of gas are in a stationary state seen from a frame rotating with the same angular velocity as the ellipsoid. (4) Magnetic lines of force are confined in the bar, and gas is good conductor.

Freeman's model of the barred galaxy, whose ellipsoidal surface is characterized by $1-(x_1^2/f_1^2)-(x_2^2/f_2^2)-(x_3^2/f_3^2)=0$, rotates with the angular velocity $\mathit{\Omega}$ with respect to an inertial system. We assume that the magnetized uniform gas is embeded in this stellar system and is bounded by an ellipsoidal surface,

$$S=1-\frac{x_1^2}{a_1^2}-\frac{x_2^2}{a_2^2}-\frac{x_3^2}{a_3^2}=0 \quad \text{with } f_i\geq a_i \quad \text{for } i=1-3.$$

The time-independent equations of motion of gas in a frame rotating with the angular velocity $\mathit{\Omega}$ are the same as Eqs. $(4\cdot1)\sim(4\cdot5)$ in §4 except that the Poisson equation for the gas can be neglected. The gravitational potential due to the stellar system is regarded as given for the motion of gas, and it is

$$\mathit{\Phi}=I-A_1x_1^2-A_2x_2^2-A_3x_3^2 \quad \text{for } 1-\frac{x_1^2}{f_1^2}-\frac{x_2^2}{f_2^2}-\frac{x_3^2}{f_3^2}\geq0, \qquad (6\cdot1)$$

in the (x_1, x_2, x_3) coordinates system, where

$$I=\frac{3}{4}GM\int\frac{ds}{\mathit{\Delta}}, \quad A_i=\frac{3}{4}GM\int\frac{ds}{(f_i^2+s)\mathit{\Delta}}$$

and

$$\mathit{\Delta}=[(f_1^2+s)(f_2^2+s)(f_3^2+s)]^{1/2}. \qquad (6\cdot2)$$

When $\boldsymbol{B}=0$, the pressure P is written as

$$P=P_cS=P_c\left(1-\frac{x_1^2}{a_1^2}-\frac{x_2^2}{a_2^2}-\frac{x_3^2}{a_3^2}\right), \qquad (6\cdot3)$$

with P_c, the pressure at the center.

We look for solutions of the velocity field and magnetic field in the following forms,

$$\boldsymbol{U}=\boldsymbol{AX} \qquad (6\cdot4)$$

and

$$\boldsymbol{B}=\boldsymbol{CX} \quad \text{for } S\geq0,$$

$$=0 \quad \text{for } S<0, \qquad (6\cdot5)$$

with the 3×3 time-independent matrices $\boldsymbol{A}$ and $\boldsymbol{C}$.

The magnetic field, $\boldsymbol{B}=0$ for $S\leq0$ and $\boldsymbol{B}\neq0$ for $S\geq0$, generates the surface current $\boldsymbol{J}_s$ which, coupled with $\boldsymbol{B}$, exerts a force $\frac{1}{2}|\boldsymbol{J}_s\times\boldsymbol{B}|$ normal to the surface and pointing outward. The pressure P in Eq. (6·3), when $\boldsymbol{B}\neq0$ and the gas is incompressible, may be written,

$$P=P_c S-\tfrac{1}{2}|\boldsymbol{J}_s\times\boldsymbol{B}|, \tag{6·6}$$

where the last term takes the form of $\sum_{ij}b_{ij}x_ix_j$, when the magnetic field (6·5) is taken.

Substitutions of Eqs. (6·4) and (6·5) in Eqs. (4·3) and (4·4), and the boundary conditions $(\boldsymbol{B}\cdot\mathrm{grad})S=(\boldsymbol{U}\cdot\mathrm{grad})S=0$ yield

$$\begin{pmatrix} U_1 \\ U_2 \\ U_3 \end{pmatrix}=\begin{pmatrix} 0 & -a_1^2\lambda_3 & a_1^2\lambda_2 \\ a_2^2\lambda_3 & 0 & -a_2^2\lambda_1 \\ -a_3^2\lambda_2 & a_3^2\lambda_1 & 0 \end{pmatrix}\begin{pmatrix} x_1 \\ x_2 \\ x_3 \end{pmatrix} \tag{6·7}$$

and

$$\begin{pmatrix} B_1 \\ B_2 \\ B_3 \end{pmatrix}=\sqrt{4\pi\rho}\begin{pmatrix} 0 & -a_1^2\mu_3 & a_1^2\mu_2 \\ a_2^2\mu_3 & 0 & -a_2^2\mu_1 \\ -a_3^2\mu_2 & a_3^2\mu_1 & 0 \end{pmatrix}\begin{pmatrix} x_1 \\ x_2 \\ x_3 \end{pmatrix}, \tag{6·8}$$

where ρ is the density of gas and the λ_j's and μ_j's are still unspecified numbers. From Eqs. (6·7), (6·8) and (4·5) we have

$$[\mathrm{rot}(\boldsymbol{U}\times\boldsymbol{B})]_i=\sqrt{4\pi\rho}\,a_i^2[a_j^2(\lambda_k\mu_i-\lambda_i\mu_k)x_k-a_k^2(\lambda_i\mu_j-\lambda_j\mu_i)x_j], \tag{6·9}$$

where the letters i, j and k are cyclic and denote 1, 2 and 3. This equation must be satisfied for $S\geq0$, or we have

$$\mu_1/\lambda_1=\mu_2/\lambda_2=\mu_3/\lambda_3, \tag{6·10}$$

which concludes that the magnetic line of force is, in a stationary state, parallel or antiparallel to the streamline of the internal motion.

Using Eqs. (6·6), (6·7) and (6·8) with (6·10), Eq. (4·1) can be written explicitly as

$$a_i^2[a_j^2(1-\varepsilon^2)\lambda_k^2+a_k^2(1-\varepsilon^2)\lambda_j^2]-2A_i+2(a_j^2\lambda_k\varOmega_k+a_k^2\lambda_j\varOmega_j)$$
$$+\varOmega_j^2+\varOmega_k^2+\frac{2P_c}{a_i^2\rho}=0, \tag{6·11}$$

$$a_i^2a_k^2(1-\varepsilon^2)\lambda_i\lambda_j+2a_k^2\varOmega_j\lambda_i+\varOmega_i\varOmega_j=0 \tag{6·12}$$

and

$$a_i^2a_j^2(1-\varepsilon^2)\lambda_i\lambda_k+2a_j^2\varOmega_k\lambda_i+\varOmega_i\varOmega_k=0, \tag{6·13}$$

where ε^2 represents the energy density ratio, $(\boldsymbol{B}^2/8\pi)/(\frac{1}{2}\rho\boldsymbol{U}^2)$, and it is constant in the gaseous ellipsoid of $S\geq0$.

In what follows, we attempt to find dynamically permissible configurations of magnetic field in the following model barred galaxy;

$$\Omega_0 = 9.1 \times 10^{-16} \text{ radians/sec}, \quad f_1:f_2:f_3 = 1:1/3:1/6, \quad \rho_* = 0.3 \, M_\odot/\text{pc}^3,$$

$$M = \tfrac{4}{3}\pi f_1 f_2 f_3 \rho_* = 3.6 \times 10^{10} M_\odot \quad \text{with} \quad f_1 = 8 \text{ kpc}. \tag{6.14}$$

The three principal axes of the gaseous ellipsoid are assumed to coincide with those of the model barred galaxy and $\boldsymbol{\Omega} = \Omega_0 \boldsymbol{e}_3$, where $\boldsymbol{e}_3$ is the unit vector of the x_3-axis. Equations $(6\cdot11) \sim (6\cdot13)$ are reduced to

$$a_1^2 a_2^2 (1-\varepsilon^2)\lambda_3^2 - 2A_1 + 2a_2^2\lambda_3\Omega_0 + \Omega_0^2 + \frac{2P_c}{a_1^2\rho} = 0, \tag{6.15}$$

$$a_1^2 a_2^2 (1-\varepsilon^2)\lambda_3^2 - 2A_2 + 2a_1^2\lambda_3\Omega_0 + \Omega_0^2 + \frac{2P_c}{a_2^2\rho} = 0, \tag{6.16}$$

$$-2A_3 \qquad\qquad + \frac{2P_c}{a_3^2\rho} = 0 \tag{6.17}$$

and

$$\lambda_1 = \lambda_2 = 0, \tag{6.18}$$

where A_1, A_2 and A_3, and Ω_0 are regarded as given. Equation $(6\cdot18)$ means that the magnetic line of force and the streamline of the internal motion are, if present, in the plane perpendicular to $\boldsymbol{\Omega}$. Elimination of P_c/ρ from Eqs. $(6\cdot15)$ and $(6\cdot16)$ gives

$$\Omega_0^2 + a_1^2 a_2^2 (1-\varepsilon^2)\lambda_3^2 = 2\frac{a_1^2 A_1 - a_2^2 A_2}{a_1^2 - a_2^2}. \tag{6.19}$$

We have six quantities to be determined, a_1, a_2, a_3, ε^2, λ_3 and $\sqrt{P_c/\rho}$, against three Eqs. $(6\cdot15) \sim (6\cdot17)$. Therefore, various ellipsoidal distributions of gas and magnetic field configurations are permitted for a given barred galaxy which is characterized by the magnitudes of Ω_0, A_1, A_2 and A_3. We shall discuss three typical cases of these various configurations in more details and compare them with observations.

(a) $\lambda_3 \neq 0$ and $1-\varepsilon^2 \neq 0$

Equation $(6\cdot19)$ yields λ_3^2 when one assumes a_1, a_2 and ε^2. The numerical values of $\pm\lambda_3$ gives, through Eqs. $(6\cdot16)$ and $(6\cdot17)$, $\sqrt{P_c/\rho}$ and a_3. Although various configurations of the gaseous ellipsoids (a_1, a_2, a_3) are permitted for $\lambda_3 \neq 0$ and $1-\varepsilon^2 \neq 0$, they have nearly the same characters concerning the internal motion and the magnetic field. A typical example is given in Fig. 16 for $a_1 = 8$ kpc, $a_2 = 1.3$ kpc and $\varepsilon^2 = 0.1$ of the gaseous ellipsoid embedded in the model barred galaxy $(6\cdot14)$. Some numerical values are listed in Table V for the two possible roots of Eq. $(6\cdot19)$ $\lambda_3 \gtrless 0$, and for $\rho = 0.5$ hydrogen atoms/cm^3, where $\lambda_3 < 0$ implies retrograde motion in the reference coordinates

system. The magnetic line of force can be both parallel and antiparallel to the streamline (Fig. 16). The internal velocity along the bar (Table V) is compatible with the observed ones (de Vaucouleurs and de Vaucouleurs 1963a and b; de Vaucouleurs 1964; and de Vaucouleurs, de Vaucouleurs and Freeman 1968), but the numerical values of $\sqrt{P_c/\rho}$ and a_3 for $\lambda_3 < 0$ seems somewhat too large.
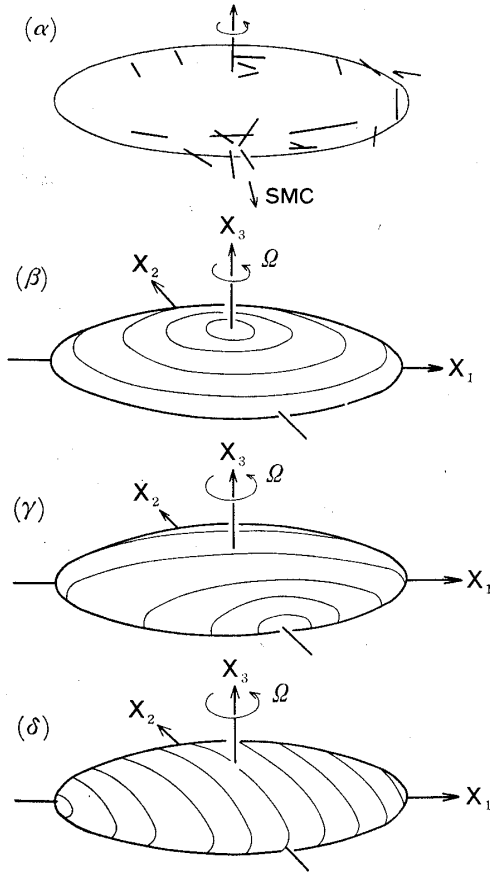
Fig. 16. Polarization planes of starlight in the bar of the Large Magellanic Cloud observed by Mathewson and Ford (1970), and calculated distributions of magnetic lines of force in models of the LMC-type barred galaxy (β to δ). If we follow Davis and Greenstein (1951), the E-vector of polarized starlight represents the direction of magnetic field projected onto the sky (α).

(β): $\lambda_3 \neq 0$, $1-\varepsilon^2 \neq 0$; $\lambda_3 \neq 0$, $1-\varepsilon^2 = 0$; $\lambda_3 = 0$, $\mu_3 \neq 0$, $\mu_1 = \mu_2 = 0$.

(γ): $\lambda_3 = 0$, $\mu_2 \neq 0$, $\mu_1 = \mu_3 = 0$.

(δ): $\lambda_3 = 0$, $\mu_1 \neq 0$, $\mu_2 = \mu_3 = 0$.

Table V.   An example for the case (a), $\lambda_3 \neq 0$ and $1-\varepsilon^2 \neq 0$.

	$a_1 = 8$ kpc, $a_2 = 1.3$ kpc, $\varepsilon^2 = 0.1$, $\rho = 0.5 H$ cm^{-3}	
λ_3	>0	<0
a_3	0. 48 kpc	1. 1
U_1	$-52 \times (x_2/1$ kpc$)$ km/sec	$+52 \times (x_2/1$ kpc$)$
U_2	$+1.4 \times (x_1/1$ kpc$)$ km/sec	$-1.4 \times (x_1/1$ kpc$)$
$\sqrt{P_c/\rho}$	33 km/sec	80
B_1	$\pm 5.5 \times (x_2/1$ kpc$) \times 10^{-6}$ gauss	$\pm 5.5 \times (x_2/1$ kpc$) \times 10^{-6}$
B_2	$\mp 0.5 \times (x_1/1$ kpc$) \times 10^{-6}$ gauss	$\mp 0.5 \times (x_1/1$ kpc$) \times 10^{-6}$
U_3 and B_3	0	0

We still do not know which is actually present, $\lambda_3 < 0$ or $\lambda_3 > 0$, in the gas of the barred galaxy. It is worth while noticing that if the barred galaxy is formed through nonaxisymmetric gravitational collapse of a rotating gaseous cloud, the internal motion of gas is always $\lambda_3 > 0$ because of the conservation of the circulation integral (Fujimoto 1968). If we observe a retrograde motion of gas $\lambda_3 < 0$ in the barred galaxy, we may conclude that the gas is not a primordial one left behind after formation of star but it has been accumulated by mass ejection of the evolved member stars and/or of the galactic nucleus.

(b) $\lambda_3 \neq 0$ and $\varepsilon^2 = 1.0$

Equation (6·19) gives the ratio,

$$\frac{a_2}{a_1} = \frac{2A_1 - \Omega_0^2}{2A_2 - \Omega_0^2} \ . \tag{6·20}$$

If we assume a magnitude of a_1, the ratio (6·20), Eqs. (6·15) and (6·17) give a relation between λ_3 and a_3,

$$\lambda_3 = (2a_1^2 A_1 - 2a_3^2 A_3 - a_1^2 \Omega_0^2) / 2a_1^2 a_2^2 \Omega_0 \ . \tag{6·21}$$

Table VI lists the numerical quantities for the case of $a_1 = 8$ kpc (therefore $a_2 = 1.7$ kpc) and $a_3 = 0.6$ kpc. The gaseous density is taken as $\rho = 0.5$ hydrogen atoms/cm^3 as before. The field intensity seems slightly too large; B_1 and B_2 are of the order of 10^{-5} gauss or more at $(a_1, 0, 0)$ and $(0, a_2, 0)$.

No noticeable difference is found between the case of $\varepsilon^2 = 1$ and that of $\varepsilon^2 = 0.1$ and $\lambda_3 > 0$ (compare the numerical values in Tables V and VI), and the magnetic field topologies in both cases are the same. Therefore, it seems not feasible to confirm observationally whether the energy equipartition $\varepsilon^2 = 1$ holds in gas of the Magellanic-type barred galaxy.

Table VI. An example for the case (b), $\lambda_3 \neq 0$ and $1 - \varepsilon^2 = 0$.

$a_1 = 8$ kpc, $\quad a_2 = 1.7$ kpc, $\quad a_3 = 0.6$ kpc, $\quad \rho = 0.5H$ cm^{-3}	
λ_3	> 0
U_1	$-55 \times (x_2/1 \text{ kpc})$ km/sec
U_2	$2.5 \times (x_1/1 \text{ kpc})$ km/sec
B_1	$\pm 1.8 \times 10^{-5} (x_2/1 \text{ kpc})$ gauss
B_2	$\mp 8 \times 10^{-6} (x_1/1 \text{ kpc})$ gauss
$\sqrt{P_c/\rho}$	60 km/sec
U_3 and B_3	0

(c) $\lambda_3 = 0$; No internal motion

When no internal motion of gas is present in the barred galaxy, we must start from the original equations of motion $(6\cdot11) \sim (6\cdot13)$ in which $\varepsilon^2 \lambda_j$ is regarded as μ_j,

$$-a_i^2(a_j^2\mu_k^2 + a_k^2\mu_j^2) - 2A_i + (1-\delta_{i3})\Omega_0^2 + \frac{2P_c}{a_i^2\rho} = 0, \qquad (6\cdot22)$$

$$a_i^2 a_k^2 \mu_i \mu_j = 0 \qquad\qquad\qquad\qquad (6\cdot23)$$

and

$$a_i^2 a_j^2 \mu_i \mu_k = 0, \qquad\qquad\qquad\qquad (6\cdot24)$$

where $\delta_{i3} = 1$ for $i = 3$ and $\delta_{i3} = 0$ otherwise. Equations $(6\cdot23)$ and $(6\cdot24)$ show that two of μ_1, μ_2 and μ_3, at least, must be zero. A case of $\mu_1 \neq 0$ and $\mu_2 = \mu_3 = 0$ is considered here for the model barred galaxy $(6\cdot14)$. (Two other cases of $\mu_2 \neq 0$, $\mu_1 = \mu_3 = 0$ and $\mu_3 \neq 0$, $\mu_1 = \mu_2 = 0$ can be treated in the same way). Equation $(6\cdot22)$ can be written explicitly when we specify μ_j's as $\mu_1 \neq 0$ and $\mu_2 = \mu_3 = 0$. Then we have five quantities to be determined, a_1, a_2, a_3, μ_1 and $\sqrt{P_c/\rho}$, against Eq. $(6\cdot22)$ for $i = 1 - 3$ as before. A magnetized gaseous ellipsoid satisfying these equations is given in Table VII for $a_1 = 8$ kpc and $a_2 = 1.3$ kpc. The magnetic field configuration is demonstrated schematically in Fig. 16 together with other two cases of $\mu_1 = \mu_3 = 0$ and $\mu_2 \neq 0$, and $\mu_1 = \mu_2 = 0$ and $\mu_3 \neq 0$.

Table VII. An example for the case (c), $\lambda_3 = 0$, $\mu_1 \neq 0$ and $\mu_2 = \mu_3 = 0$.

$a_1 = 8$ kpc, $a_2 = 1.3$ kpc, $\rho = 0.5\,H\,\mathrm{cm}^{-3}$	
a_3	1 kpc
B_2	$\pm 2.3 \times 10^{-5}(x_3/1\,\mathrm{kpc})$ gauss
B_3	$\mp 1.3 \times 10^{-6}(x_2/1\,\mathrm{kpc})$ gauss
$\sqrt{P_c/\rho}$	79 km/sec
U_1, U_2, U_3, B_1	0

6-2 *Comparisons with observations*

The three cases (a) $\sim$ (c) in the previous subsections represent qualitatively all permissible configurations of stream lines of gas and magnetic fields in the Freeman's barred galaxy. They are illustrated in Fig. 16, together with the magnetic field distribution in the bar of the LMC estimated from the optical polarization measurements of stars (Mathewson and Ford 1970). Making a comparison between the field topologies $(\alpha) \sim (\delta)$, we find that the case (c) of $\lambda_3 = 0$, $\mu_1 \neq 0$ and $\mu_2 = \mu_3 = 0$ seems to be ruled out, because this case cannot account for the observed topology of the magnetic field in the bar. Moreover it is necessary to remind us that the internal motion

of gas has been confirmed in the Magellanic-type barred galaxy (de Vaucouleurs and de Vaucouleurs 1963 a and b; de Vaucouleurs 1964; and de Vaucouleurs, de Vaucouleurs and Freeman 1968) which is incompatible with the case of $\lambda_3 = 0$.

The other two cases (a) and (b) seem preferable to represent the observed field topology, although the case (b) permits the internal motion only of $\lambda_3 > 0$. The internal motion of gas in some Magellanic-type barred galaxies, $\lambda_3 \neq 0$, has been confirmed, but we do not have observationally definite knowledge about the sign of λ_3. More observational material must be accumulated, in order to determine which is more appropriate, the case (a) or (b), to describe the characteristic distribution of the magnetic field in the bar.

We may conclude from these facts that the magnetic field configuration observed by Visvanathan (1966) and Mathewson and Ford (1970) is explained qualitatively in terms of a large-scale internal motion of gas so far as the magnetic field in the bar is concerned, although it is not clear whether this circulation is characterized by $\lambda_3 > 0$ or $\lambda_3 < 0$ (retrograde).

Schmidt (1970) has found a large-scale panmagellanic magnetic field in a gigantic space enveloping both the LMC and the SMC. It is a remarkable fact that the magnetic lines of force in this space are aligned along the direction joining the LMC and the SMC. We cannot explain such a characteristic feature only by a convetional treatment of the tidal effect between the nebulae, or by the magneto-hydrodynamical method so far used. Presumably a new idea must be introduced in the gigantic magnetized gas cloud in which the LMC and the SMC are embedded.

References

Alfvén, H., Rev. Mod. Phys. **37** (1965), 652.

Becker, W. and Contopoulos, G., *IAU Symposium* (1970), No. 38, pp. 303~422.

Behr, A., Veröff. U. Sternw. Göttingen (1959), No. 126.

Berge, G. L. and Seielstad, G. A., Astrophys. J. **148** (1967), 367.

Bingham, R. G. and Shakeshaft, J. R., Month. Notices Roy. Astron. Soc. **136** (1967), 347.

Bleeker, J. A. M., Burger, J. J., Deerenberg, A. J. M., Scheepmaker, A., Swanenburg, B. N., Tanaka, Y., Hayakawa, S., Makino, F. and Ogawa, H., Can. J. Phys. **46** (1968), 461.

Bolton, J. G. and Ekers, J., Austr. J. Phys. **19** (1966), 559; **20** (1967), 109.

Bolton, J. G. and Kinman, T. D., Astrophys. J. **145** (1966), 951.

Brecher, K. and Blumenthal, G. R., Astrophys. Letters **6** (1970), 169.

Burbidge, E. M., Ann. Rev. Astron. Astrophys. **5** (1967a), 399; Astrophys. J. **149** (1967a), L51.

Burton, W. B.. Astron. Astrophys. Suppl. **2** (1970), 261.

Chandrasekhar, S. and Fermi, E., Astrophys. J. **118** (1953), 116.

Cooper, B. F. C. and Price, R. M., Nature **195** (1962), 1084.

Cowling, T. G., Month. Notices Roy. Astron. Soc. **94** (1945), 39; *The Sun*, ed. G. P. Kuiper (University of Chicago Press, Chicago, 1953), p. 575.

Davis, L. and Greenstein, J. L., Astrophys. J. **114** (1951), 206.

de Vaucouleurs, G. and de Vaucouleurs, A., Astrophys. J. **137** (1963), 363.

de Vaucouleurs, G., *IAU-URSI Symposium* (1964), No. 20, p. 269.

de Vaucouleurs, G., de Vaucouleurs, A. and Freeman, K. C., Month. Notices Roy. Astron. Soc. **139** (1968), 425.

Doroshkevich, A. G., Astrofizika. **1** (1965), 255.

Evans, D. S., Observatory **87** (1967), 224.

Felten, J. E. and Morrison, P., Astrophys. J. **146** (1966), 686.

Freeman, K. C., Month. Notices Roy. Astron. Soc. **130** (1965), 183; **134** (1966), 1.

Fujimoto, M., Publ. Astron. Soc. Japan **15** (1963), 107; Astrophys. J. **152** (1968), 523.

Fujimoto, M. and Miyamoto, M., Publ. Astron. Soc. Japan **21** (1969), 194; *IAU Symposium* (1970), No. 38, p. 440.

Fujimoto, M. and Tanahashi, Y., Publ. Astron. Soc. Japan **23** (1971), 7.

Gardner, F. F. and Whiteoak, J. B., Nature **197** (1963), 1162.

Gardner, F. F., *IAU-URSI Symposium* (1964), No. 20 (Sydney-Canbera), p. 143.

Gardner, F. F. and Davies, R. D., Austr. J. Phys. **19** (1966), 129.

Gardner, F. F., Whiteoak, J. B. and Morris, D., Nature **214** (1967), 371; Austr. J. Phys. **22** (1969), 79, 821.

Ginzburg, V. L. and Syrovatskii, S. I., *The Origin of Cosmic Rays* (Pergamon Press, 1964), Chap. III, p. 241.

Harrison, E. R., Phys. Rev. Letters **18** (1967), 1011.

Hiltner, W. A., Astrophys. J. **109** (1949), 471; **114** (1951), 241; Astrophys. J. Suppl. **2** (1956), 381.

Hornby, J. M., Month. Notices Roy. Astron. Soc. **133** (1966), 213.

Hoyle, F. and Ireland, J. G., Month. Notices Roy. Astron. Soc. **122** (1961), 35.

Humason, M. L., Mayall, N. U. and Sandage, A. R., Astron. J. **61** (1956), 97.

Ireland, J. G., Month. Notices Roy. Astron. Soc. **122** (1961), 461.

Jokipii, J. R., and Lerche, I., Astrophys. J. **157** (1969), 1137.

Kawabata, K., Fujimoto, M., Sofue, Y. and Fukui, M., Publ. Astron. Soc. Japan **21** (1969), 293.

Kerr, F. J., Austr. J. Phys. Astrophys. Suppl. No. 9 (1969), 1; *IAU Symposium* (1970), No. 38, p. 95.

Lamb, H., *Hydrodynamics* (Dover Publications, New York, 1945), Chap. XII.

Lin C. C. and Shu, F. H., Astrophys. J. **140** (1964), 646.

Lindblad, P. O., Bull. Astron. Inst. Netherl. **19** (1967), 34.

Matthews, T. A., Morgan, W. W. and Schmidt, M., Astrophys. J. **140** (1964), 35.

Mathewson, D. S., Astrophys. J. **153** (1968), L47.

Mathewson, D. S. and Nicholls, D. C., Astrophys. J. **154** (1968), L11.

Mathewson, D. S. and Ford, V. L., Astrophys. J. **160** (1970), L43; Astron. J. **75** (1970), 778.

Morris, D. and Berge, G. L., Astrophys. J. **139** (1964), 1388.

Omnés, R., Phys. Rev. Letters **23** (1969), 38; Phys. Rev. **D1** (1970), 723.

Oort, J. H., *La structure et l'evolution de l'univers* (Brussels, Stoops, 1958), p. 163; *Stars and Stellar Systems*, eds. A. Blaauw and M. Schmidt (University of Chicago Press, Chicago), Vol. 5 (1965), Chap. 21.

Parker, E. N., Astrophys. J. **157** (1969), 1129.

Prendergast, K. H., *Interstellar Matter in Galaxies*, ed. L. Woltjer (W. A. Benjamin, Inc., 1962), p. 217.

Reinhardt, M., Astrophys. Letters **8** (1971a), 155; **8** (1971b), 181.

Reinhardt, M. and Thiel, M. A. F., Astrophys. Letters **7** (1970), 101.

Rougoor, G. W., Bull. Astron. Inst. Netherl. **17** (1964), 381.

Sandage, A. R., Astrophys. J. **145** (1966), 1; **150** (1967), L145.

Schmidt, M., *Stars and Stellar Systems*, eds. A. Blaauw and M. Schmidt (University of Chicago Press, Chicago), Vol. 5 (1965), Chap. 22; Astrophys. J. **141** (1965), 1.

Schmidt, M. and Matthews, T. A., Astrophys. J. **139** (1964), 781.

Schmidt, Th., Astron. Astrophys. **6** (1970), 294.

Shajn, G. A., Soviet Astron.-AJ **33** (1956), 469.

Sofue, Y., Fujimoto, M. and Kawabata, K., Publ. Astron. Soc. Japan **20** (1968), 388.

Stępień, K., Acta Astron. **14** (1964), 81.

Tadokoro, M., Publ. Astron. Soc. Japan. **20** (1968), 230.

Thorne, K. S., Astrophys. J. **148** (1967), 51.

Turtle, A. J. and Baldwin, J. E., Month. Notices Roy. Astron. Soc. **124** (1962), 459.

Velden, L., *IAU Symposium* (1970), No. 38, p. 164.

Visvanathan, N., Month. Notices Roy. Astron. Soc. **132** (1966), 432.

Westerhout, G., *Maryland-Green Bank Galactic 21-cm Line Survey* (University of Maryland 1966, 1969), 1st and 2nd editions.

Zel'dovich, Ya. B., JETP **48** (1965), 986.